High-speed atomic force microscopy for materials science

O. D. Payton*[1,2], L. Picco[1] and T. B. Scott[1]

[1] Interface Analysis Centre, School of Physics, H.H. Wills Physics Laboratory,University of Bristol, Tyndall Avenue BS8 1TL, UK
[2] Engineering Maths, Merchant Venturers School of Engineering, University of Bristol, Merchant Venturers' Building, Woodland Road, Clifton BS8 1UB,UK
*Corresponding author, email Oliverdpayton@gmail.com

Abstract

Since its inception in 1986, the field of atomic force microscopy (AFM) has enabled surface analysis and characterisation with unparalleled resolution in a wide variety of environments. However, the technique is limited by very low sample throughput and temporal resolution making it impractical for materials science research on macro sized or time evolving samples such as the observation of corrosion. The potential of AFM sparked intense efforts to overcome these limitations shortly after its invention, and has led to the development of high-speed atomic force microscopes (HS-AFMs). Within the last 5 years the technology underpinning these instruments has matured to the point where routine imaging can achieve megapixels per second over scan areas of square millimetres, removing the limitations from AFM for industrial scale materials characterisation. This review explains the technology and looks to the future use of HS-AFMs in materials science.

Introduction

Research in materials science often requires in-depth characterisation of bulk and surface properties of samples from measuring the size distribution of nanoparticles to assessing impurities in steel, or performing quality assessment on a batch of fabricated nanostructures. This array of applications call for a suite of appropriate tools. The scanning electron microscope (SEM) is currently the gold standard in surface topography mapping for materials science at the macro to the microscale. At the nanoscale however, materials science lacks a suitable tool that offers rapid, accurate materials surface analysis over large areas.

Atomic force microscopy[1] has historically excelled at nanoscale imaging,[2] but has been most popular for biological studies only due to the small sample size and slow data-collection time. It has, as a technique, much to offer materials scientists, were this size and speed limitation addressed. A key benefit is that it is not limited, unlike SEM, to vacuum or low pressure environments; atomic force microscopy (AFM) is able to image well in gaseous or liquid environments. The sample preparation is non-destructive and quick, and the resolution at the nanoscale is such that atomic and sub-atomic features can be resolved.

High-speed AFM (HS-AFM) can offer the same resolution and imaging environment benefits as traditional AFM to materials scientists at a vastly improved rate of data collection. HS-AFM provides a complementary technique to existing toolsets and in most cases surpasses SEM in terms of resolution. HS-AFM also offers new functionality over traditional AFM in the ability to observe processes, in real-time. This is functionality that is simply unavailable with SEM and can offer extremely valuable insight into how processes catalyse and progress. HS-AFM also offers large-scale imaging of areas millimetre or centimetre squared in size as discussed later. Figure 1 shows how the imaging speeds of various surface characterisation tools compare. This review will introduce the field of atomic force microscopy and detail the advantages high-speed AFMs can offer materials science.

Many SEMs have a resolution stated in the region a few nanometres, some SEMs may even have sub-nanometre lateral resolution[3] and will typically take a minute to collect an image 2 µm across at this resolution. Although SEMs and AFMs can produce images which at first glance look similar it is important to understand that the tools are complimentary in nature.[4–6] An AFM will produce a three dimensional map of the sample topography of the surface with sub-nanometre lateral resolution and sub-angstrom height resolution, but is limited to imaging features which are bound to the sample surface and with a very low aspect ratio (in the order of 100s of nanometres height change per micron). Whereas SEMs are capable of collecting a two dimensional image of samples with a high aspect ratio. While AFMs image just the surface of a sample (with the exception of a few specialised imaging modes) an SEM has

an interaction volume[7] associated with each pixel measured, this ultimately allows AFMs to exceed the resolution of SEMs.[8]

Overview of atomic force microscopy

In this review, the various HS-AFMs that have been developed to date will be discussed in terms of their potential and reported applications to materials science. It is necessary to first understand the main AFM imaging modes and the key hardware elements underpinning the technique.

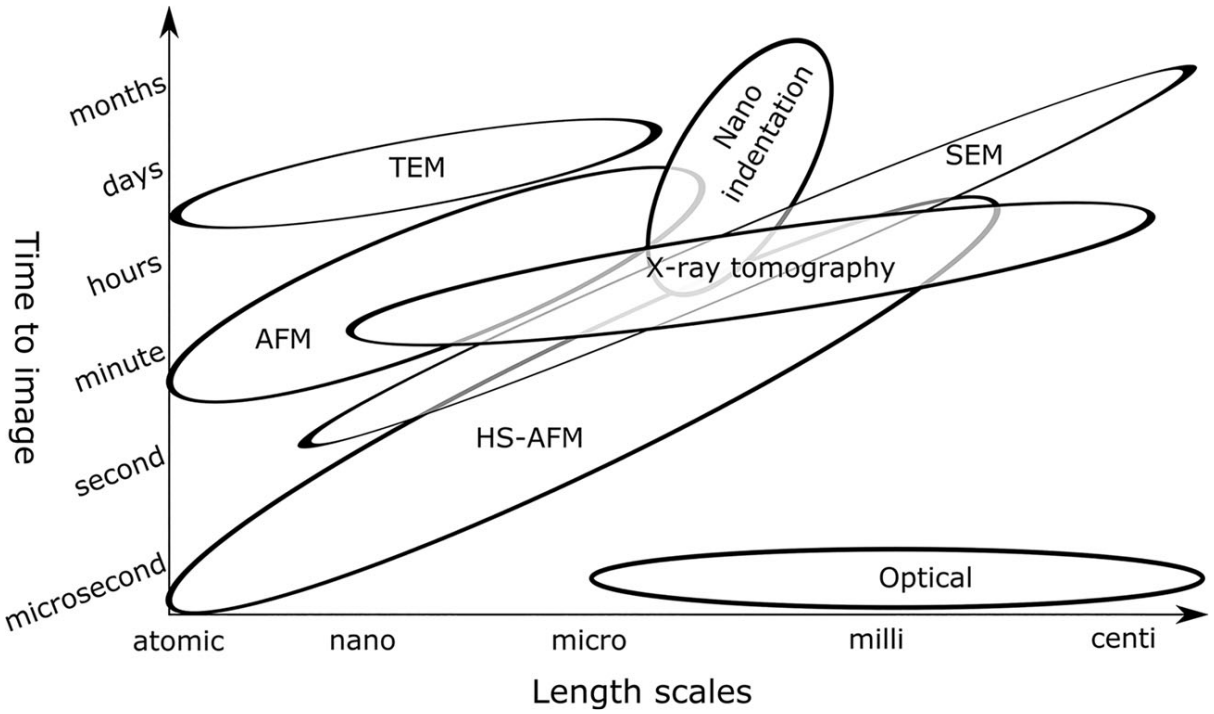

Figure 1 Schematic graph plotting how various surface characterisation techniques compare in terms of imaging speeds and image size while maintaining the highest achievable resolution for each tool. © [Payton]

AFM is a member of a large family of related techniques collectively known as scanning probe microscopy (SPM). Other notable members include scanning tunnelling microscopy,[9,10] near-field scanning optical microscopy[11] and scanning ion-conductance microscopy.[12] The common feature that these diverse techniques share is that they all obtain high spatial resolution measurements by raster-scanning a probe with a sharp (less than 10 nm radius) detection tip across the sample surface. The detection tip localises the interaction between the probe and the sample, enabling extremely high-resolution images to be obtained.[13] Figure 2 shows a schematic illustrating the basic operating principles of AFM. Alternative scanning patterns may be used, such as the spiral[14,15] or Lissajous[16–18] in order to avoid the high fast scan frequency necessary to build up the raster scan. However, due to the ease of reconstructing the resulting image in software the raster scan is still the most commonly used scan pattern.

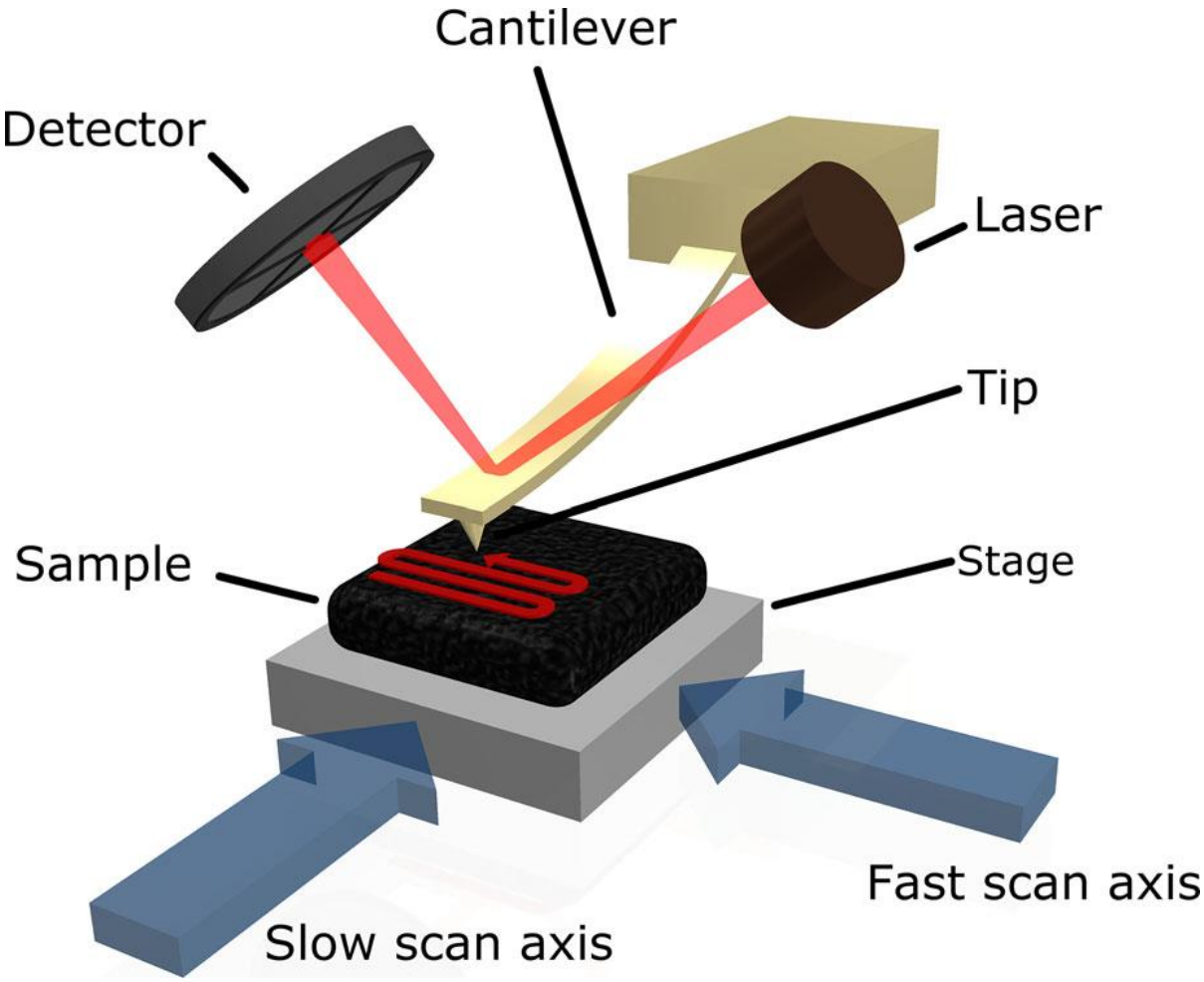

Figure 2 Schematic diagram of a simple AFM. The cantilever's response to the surface is mapped as the sample is moved under the sharp cantilever tip in a raster pattern. An AFM cantilever is typically 100–300 µm in length. © [Payton]

AFM imaging modes

To measure the topography and other properties of the sample, the probe must be moved from pixel-to-pixel in a serial fashion. To control the interaction force between the probe and sample and prevent either wear of the detection tip or damage to the sample, an electronic control loop is typically used to maintain a constant probe–sample interaction force. There are several schemes for how this control loop can be implemented to control the behaviour of the probe during scanning and the main three methods imaging modes in AFM have been named after them. They are: contact mode[19]; intermittent contact mode[20,21] (also known as tapping mode) and; non-contact mode.[22]

Contact mode

Contact mode was the imaging mode of the original atomic force microscope[1] and uses the simplest control system. In contact mode, the probe is held in continuous contact with the sample surface during scanning. In this mode, the force exerted on the sample by the tip of the probe is controlled by monitoring the deflection angle of the cantilever beam and raising or lowering the probe to maintain a pre-selected deflection. In order to minimise the interaction force normal to the sample surface contact mode, probes are typically designed and fabricated from silicon nitride such that the cantilever beam has a very low spring constant (commonly between 0.006 and 1 N m^{-1}). This minimises the likelihood that the tip of the probe will deform or damage the sample surface. However, because the tip remains in contact with the sample throughout scanning there are often large lateral interaction forces[23–26] which can lead to loosely bound or delicate samples being swept during imaging.[27,28]

Intermittent contact mode

Intermittent contact mode was developed in response to a growing interest in studying biological molecules and systems with AFM. During intermittent contact mode imaging, the probe is oscillated at its fundamental resonance frequency and the detection tip 'taps' the sample at one end of each oscillation. A lock-in amplifier monitors the amplitude of this oscillation (typically between 10 and 100 nm)[29] and raises or lowers the probe to maintain a pre-set amplitude. This results in shorter probe–sample contact times and reduced lateral interaction forces at the expense of increased normal interaction forces. The lower lateral forces enable intermittent contact mode AFM to excel at imaging fragile biological samples.

Non-contact mode

The third imaging mode requires the most complex and sensitive control system. In non-contact mode the probe is oscillated with much smaller amplitudes (10 nm or less) than intermittent contact mode which allows longrange van der Waals interaction forces between the probe and the sample to be sensed and used to prevent probe–sample contact.[22,30,31] Due to the small margins for error in oscillating the probe close to but, without touching the sample, successful non-contact imaging requires an extremely sensitive detection system and a fast control loop to maintain the correct probe–sample separation. Good thermal and acoustic isolation of the instrument from the environment are also critical. Noncontact mode exerts the least lateral or normal forces on the sample and is very useful for measurements requiring the highest sensitivity and delicacy.[13,22,32,33]

Key AFM hardware elements

The main factor that has stunted the growth of use of AFMs in material science is its imaging speed. It typically takes minutes to collect a single frame as the mechanical and electrical components of the microscope must move the cantilever across the sample surface in order to build up an image. HS-AFM designs have improved the bandwidth of each component of the AFM to allow a substantial increase in the pixel rate of the device as shown in Table 1. The following sections detail each AFM component and explain how the design can be altered to bring them up to speed.

Probe design

The cantilever is the only AFM consumable and the development of batch processing methods for fabricating large numbers of cantilevers at low cost[34–36] was pivotal to the growing popularity of AFM.[37–41] Typically, the probe will be made of silicon or silicon nitride. It will consist of a micro-fabricated cantilever beam with a sharp (usually etched) detection tip located at its free end. AFM probes can be used in liquid or gaseous environments without alteration, though the design considerations of the cantilever, its physical dimensions and material properties vary depending on the AFM imaging mode it is to be used for. Probes intended for either intermittent contact or non-contact mode are significantly different from those used in contact mode. Contact mode cantilevers tend to be hundreds of microns in length with a fundamental resonant frequency of less than 10 kHz, while intermittent contact mode cantilevers have a first resonance over 300 kHz. The control system for both imaging modes measures the amplitude of the probe oscillation and is therefore limited in its response speed by the frequency of the oscillation. This makes probes with high (300 kHz or greater) resonant frequencies very desirable so that the number of pixels measured per second is high (500 s^{-1} or greater) and imaging times remain small (10 minutes or less for a typical 512 × 512 image).[42–46]

Detection system

Numerous detection systems have been developed to measure the motion of the cantilever. By far the most popular is an optical method commonly referred to as optical beam deflection[47–49] (see Fig. 2) because it is easy to

implement using relatively inexpensive components. Other detection systems include: optical interferometer, [50–52] laser Doppler vibrometer,[53–55] astigmatic optical systems,[56–59] as well as non-optical methods such as incorporating a piezoelectric strain gauge into the probe during fabrication.[52,60,61] The typical characteristics required of an appropriate detection system for a conventional atomic force microscope are: a bandwidth greater than 1 MHz and a sub-nm sensitivity to displacements and deflections of the cantilever beam of the probe.

Controlling the probe–sample interaction

The measurements of the deflection of the probe are input into a feedback loop[62–65] (a proportional integral differential loop[66]) along with a user-specified setpoint value of deflection angle, oscillation amplitude or frequency that should be maintained. The speed at which the feedback loop runs is determined by the speed of the slowest component in it.[66] First there is the bandwidth of the detection system at the input, then the speed of the PID loop itself and then finally the speed at which the PID output value can be turned into a physical motion of the probe to keep the interaction force at the setpoint. Large amounts of work have been done to increase and optimise the overall bandwidth of the feedback loop in order to make high-speed atomic force microscopes.[66] Contact mode has the fastest feedback loop[67] as each time step in the loop does not require the cantilever to make at least one period of oscillation before the measured signal can be acted upon, as is the case with intermittent and non-contact modes. Instead the feedback loop can be fed the cantilevers response to the surface as fast as the detection system allows.

Scan stage design

The final hardware elements are the XYZ positioning stages responsible for translating the probe relative to the sample surface. These must be capable of small steps (sub-nm in some cases) and fast linear motions. Typically, piezoelectric actuators are used in conjunction with various mechanical assemblies such as flexure stages[74–76] to create stable, smooth motions with negligible out-of plane vibrations and errors. The faster the stage can move in the fast scan direction (see Fig. 2), the more lines can be collected per second leading to a smaller pixel size and hence better resolution. The faster the stage can move in the slow scan direction then the higher the frame rate of the AFM. The speed the stage can move at will be limited to the stiffness of the stage, the speed at which the actuators can exert a sufficient force and the resonance frequency of the stage. Measuring and understanding the positional errors of AFM scan stages is essential for correct interpretation and analysis of AFM images and is especially important when mosaicking many AFM images to create large, high-resolution composite images.[77,78]

Table 1 Shows a comparison of typical bandwidths of the key components in a traditional AFM and a high-speed AFM, the *shaded boxes indicate the current bandwidth limiting component*

Hardware component	Standard intermittent contact AFM	Standard contact mode AFM	High-speed intermittent contact AFM	High-speed contact mode AFM
Cantilever	285 kHz[68]	10 kHz[69]	2 MHz[70]	10 kHz[69]
Detection system	2 MHz[71]	2 MHz[71]	2 MHz[71]	25 MHz[53]
Control system and Z actuator	10 kHz[71]	10 kHz[71]	150 kHz[72,73]	Physical limit not discovered
XY stage	10 lines per second[71]	10 lines per second[71]	15 k lines per second[73]	1–100 k lines per second[67]

Limitations on sample type

The probe is easily contaminated with loose material from the surface or surrounding medium. This adversely effects the radius of the tip, reducing the spatial resolution of the measurements and potentially introducing a variety of tip shape induced image artefacts (double tip, tip convolution, etc.).[79] The tip can also lose resolution through tip wear.[80]

AFMs cannot measure the shape of the sample obscured by overhangs or down the sides of vertical structures. This is because the detection tip of the probe cannot change the angle with which it approaches the sample surface. The AFMs strength is in mapping a sample surface texture on relatively flat surfaces. They are not capable of imaging surfaces with large changes in height, these samples are best imaged in an SEM.

Defining the ‘speed’ of an atomic force microscope

The speed of an atomic force microscope can be measured in many different ways. In this review ‘speed’ refers to the number of meaningful pixels collected per second by the device. By meaningful we mean pixels collected at a rate lower than or equal to the lowest bandwidth of the complete system so that the surface is not oversampled.

Other ways that the 'speed' of an AFM can be measured are the scan speed of the fast scan or the number of frames per second imaging rate; both of these are not fair measurements of speed as the lateral resolution of the resulting image often scales very poorly with an increase in scan speed due to a limited pixel rate. It is therefore fairer to measure speed in pixels per second. As will be mentioned in the following section, an increase in speed allows an increase in image rate without a loss in lateral resolution.

Materials applications

Due to the speed limitation of conventional AFMs, it did not take long before HS-AFMs were being developed. The first attempt at creating a HS-AFM was by Barrett and Quate in 1991[81] and since then the greatest driving force in the development of HS-AFMs has been from the field of biology. AFM rapidly became a popular and successful tool for biological studies because of its ability to image molecular systems under their natural physiological environmental conditions. However, while it was capable of generating high-resolution images of single molecules the low temporal resolution of conventional AFM prevented biomolecular interactions (which typically occur on second or sub-second timescales) from being observed and studied. Numerous research groups began developing HS-AFM technologies to overcome this limitation and enable these molecular interactions to be measured directly.[82,83]

Although the development of HS-AFMs has been primarily for use on biological samples, they have found a use in material science applications due to their unique spatial or temporal resolution. Some groups have now designed HS-AFMs specifically for material science research. The following sections will discuss the various HS-AFMs that have been developed in the context of their materials science applications. These examples have been placed into four topics highlighting the strengths of the tool for; observing processes, imaging large areas, mapping different material properties as well as height, and manipulating and fabricating nanostructures via HS-AFM.

Observing dynamic events

Historically, as explained above, the most common objective when developing a HS-AFM was to enable researchers to observe fast (events that occur in minutes to milliseconds rather than tens of minutes or hours) nanoscale processes directly. Conventional AFMs would provide, at best, a time lapse but may be incapable of doing anything more than capturing before and after images from which the mechanism of the process must then be inferred. If the process can be repeatedly started and stopped externally,[84] or dramatically slowed, then a conventional AFM can be used to create 'snapshots' of the surface during the process.[85–89] However, many processes cannot be controlled with this level of precision, necessitating the use of a HS-AFM.

Single molecule interactions

One group above all others has pushed the boundary forward in terms of the capability of HS-AFM. The work of Ando et al. at Kanazawa has produced a suite of HS-AFMs capable of observing nanoscale biological processes in real-time[90–94] with 0.16 megapixels per second[72] and 100 ms per frame with a scan area of 113.6 × 113.6 nm.[95] Throughout the biological AFM community this is a popular type of HS-AFM and has spearheaded the popularity of HS-AFMs globally. Although capable of imaging in high-speed contact mode Ando's HS-AFMs are best known for the observation of biological events in real time using intermittent contact mode. Every aspect of Ando's HS-AFM was optimised[66,96–99] to achieve the greatest possible imaging rate while keeping the probe–sample interaction forces at the extremely low levels required to image these delicate biological systems successfully and without damaging them. Figure 3 shows select frames from a video collected using the Kanazawa intermittent contact HS-AFM.

In order to collect the data shown in Fig. 3 custom small cantilevers with resonances 600 kHz in water[100] were designed and manufactured. A detection system with a bandwidth capable of measuring this high resonant frequency was developed[91] and a complex control system was implemented[66] which is capable of altering the cantilever– surface separation every half period of oscillation of the cantilever, thus doubling the bandwidth of the HS-AFM. A sample stage was built that was able to move the sample in the XY and Z axis with bandwidth necessary to achieve the specification previously described. Although these alterations to the design of a standard AFM has produced a world leading tool in terms of low forces on the sample they have introduced some severe limitations on the size and type of samples which can be imaged. The sample volume must be less than 1 mm^3 and the area covered by each frame has only recently improved from ~113.6 × 113.6 nm to 40 × 40 μm.[101] There are still limitations on how far this scan window can be moved, thus preventing large area maps from being made.

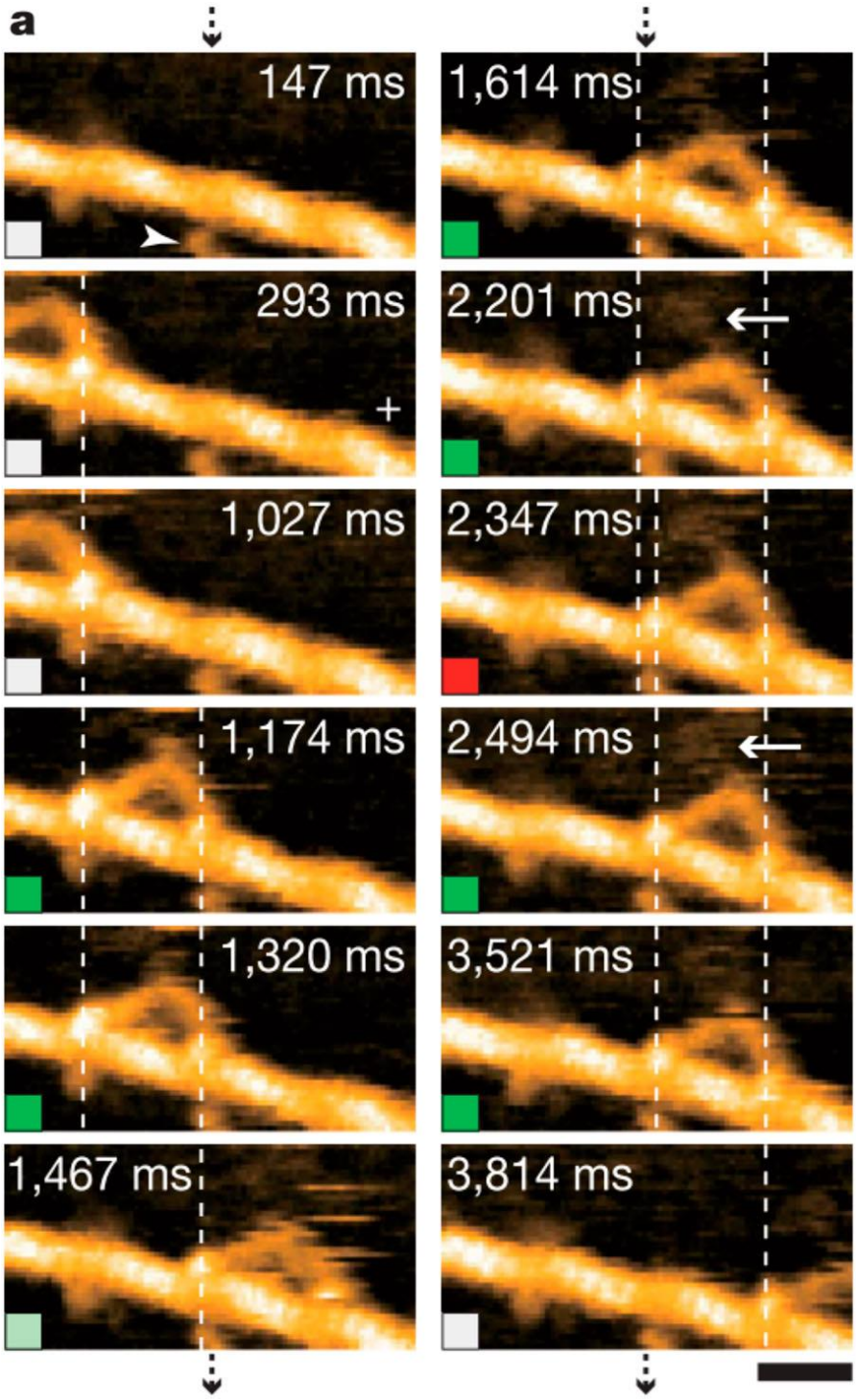

Figure 3 Selected frames form Kodera et al.[102] showing the motion of a single myosin 5 molecule 'walking' along an actin filament. The scale bar shown is 30 nm.

One of the biggest drivers for the development of HS-AFMs was to obtain single molecule behaviour at video-rate for the purposes of elucidating biological systems. The research of Ando et al. has been centred on this field, and has resulted in a device capable of observing, in real-time, the motion of molecules.[90,98,102–104] Figure 3 shows a myosin-V molecule ~5 nm is size 'walking' along an actin filament with a gait of 36 nm.[105] This is the process that transports vesicles and organelles within cells.[106] Although the process had been studied using optical traps previously,[104] the observation of the dynamic molecule lead to a more detailed understanding of the processes involved.

Although the work of Ando et al. is primarily on biological samples, it is not hard to see that the exquisite spatial resolution and force control of the technique is readily available for transfer into the field of material science. Indeed

the Ando HS-AFM is beginning to be used to monitor the dissolution of photoresists for the next generation of lithographic technologies.[107,108]

Dissolution of crystalline structures

Continuing along the theme of dissolution; the high frame rates of HS-AFM has been used to observe the dissolution of crystalline nano or micro-structures in real time. These videos can provide materials science researchers with new insights into the process with millisecond temporal resolution. Without HS-AFM the dynamics of temporally evolving systems can only be extracted from bulk measurements such as titration reactions.[109] However these experiments do not give any information about the physical process occurring on the sample surface. Standard AFMs or SEMs can provide pre- and post-data which may be used to infer a process[110] however a HS-AFM mapping the surface within an in vivo environment can provide the full story.

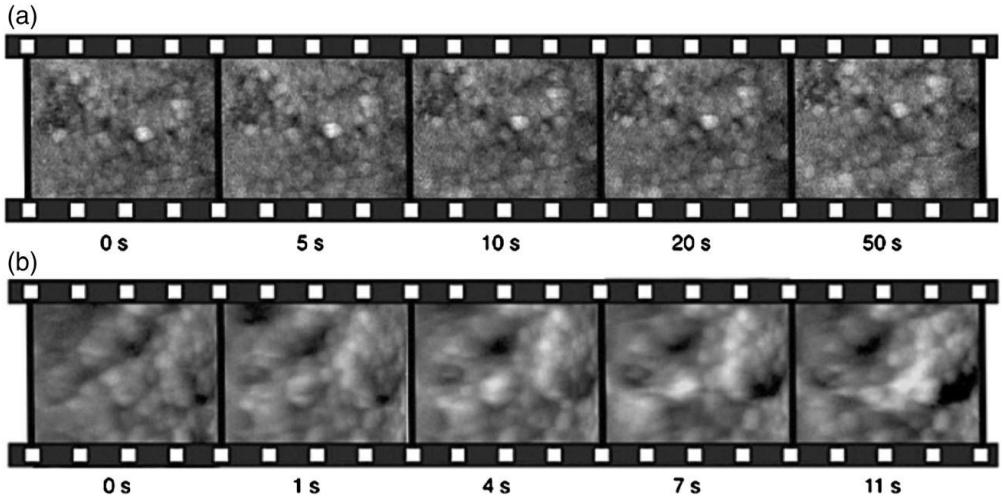

Figure 4 Selected frames, with time stamps in seconds displayed, from a HS-AFM video captured by Pyne et al.[111] The video recorded the dissolution of hydroxyapatite in a buffer solution a (3 × 3 µm), and in an acidic solution b (1.5 × 1.5 µm). Crystal dissolution can be seen in b but not a

Pyne et al. have investigated the effect of fluoride treatment on the dissolution rates of hydroxyapatite (dental tooth enamel) crystals under acidic environments.[111] They used the Bristol contact mode HS-AFM with fluid flow through cell (see Fig. 4) and compared the measured dissolution of hydroxyapatite. This showed significant spatial variation of dissolution rates across the sample, which is attributed to the extremely heterogeneous nature of natural hydroxyapatite. In addition, they reported a pronounced reduction in dissolution rate for the fluoride treated enamel.

The Bristol contact mode HS-AFM[112] makes use of a passive physical control loop[113] and uses the displacement of the cantilever above the tip[49,53,54] to map the surface topography. In the absence of a 'per pixel' control loop the device is able to operate at megapixels per second.[67] Another example is the dissolution of calcite crystals,[45 as] shown in Fig. 5. Brausmann et al. makes use of a parallel- kinematic piezo based flexure stage[74,75] that is capable of imaging samples up to 23 × 23 µm images at 10 frames per second. This particular HS-AFM makes use of small (20 µm long) cantilevers operating in conventional contact mode.

The dissolution of Calcite had been reported previously by Hillner et al.[89] at 22 seconds per frame, and Paloczi et al.[43] at 1.2 seconds per frame. With each increase in imaging speed and frame rate the dynamics of the process is shown in more detail. Brausmann's data in Fig. 5 for example shows a layer of calcite dissolving in 1.4 seconds, if imaged at lower rates this dissolution would not be recorded accurately as much of the calcite would have dissolved before the image had finished being collected. That is to say one end of the image would show the calcite layer intact while the opposite end would show it dissolved. It is important to have a frame rate faster than the dynamics you wish to observe. In order to maintain the spatial resolution required, a HS-AFM is therefore needed.

By observing material dissolution with nanoscale resolution, HS-AFM have demonstrated how inhomogeneous the process of dissolution of the sample surface is. It is also clear that the macro scale observation of the dissolution process is controlled by the structures present at the nanoscale, and only observable directly using HS-AFM.

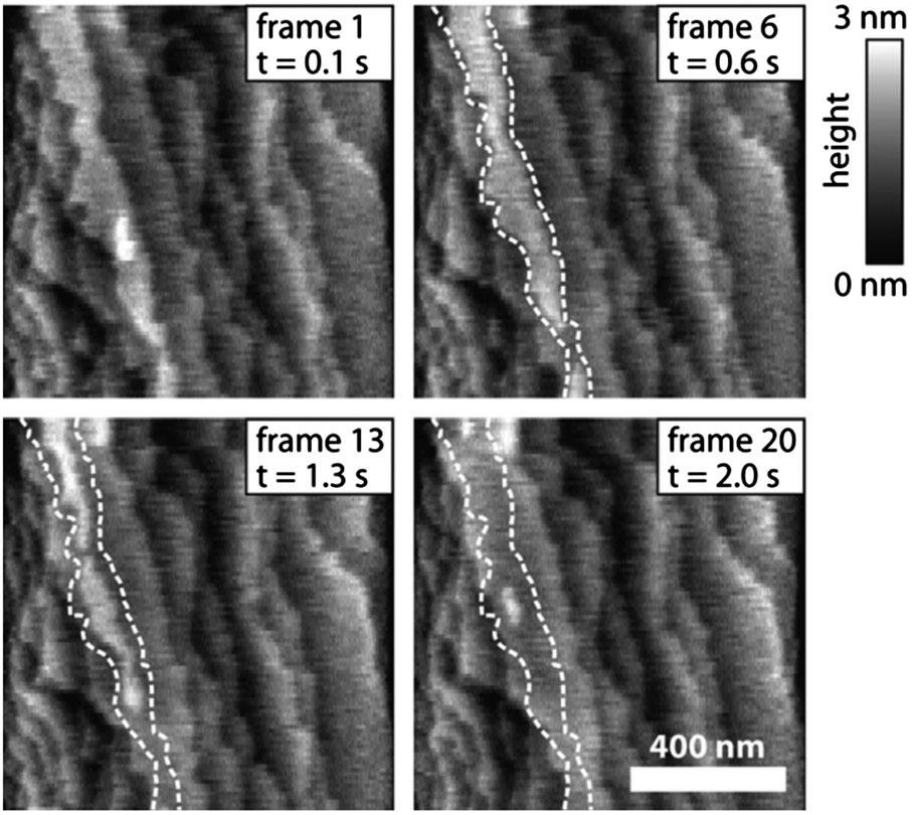

Figure 5 Selected fames from a HS-AFM video collected by Braunsmann et al.[45] Over the course of 2 s the dissolution of Calcite crystals is observed.

Magnesium chloride crystallisation

The formation of nano and micro structures can be observed in a similar fashion. The following example of crystallisation was observed during a study[114] that aimed to optimise the magnesium chloride concentration in a DNA buffer solution. It is a good indicator of the capability of HS-AFM to observe nucleation and measure growth rates.[115] The large area imaging capability of the HS-AFM is as important as the fast imaging and high resolution in this case as it is difficult to predict where the nucleation sites might be. If they are disperse on the sample a technique that can find these rare features quickly is needed.

It was found that at high magnesium chloride concentrations the two dimensional crystals formed and their growth could be observed via a contact mode HS-AFM as shown in Fig. 6.

Provided sufficient ambient humidity is present the magnesium chloride crystals were found to form spontaneously. Within the field of metallurgy, the growth of salt crystals on a surface can be the first step towards the corrosion of that material.[116–119] However, it was also found that the action of imaging the sample surface was also enough to initiate the crystallisation process. Once nucleated, the crystals were found to continue to grow until the whole mica surface was covered. Although crystal growth was also observed in areas which were not imaged, using a HS-AFM, as with any other SPM, carries the risk of interfering with the sample dynamics and this must be taken into account when planning experimental observations.

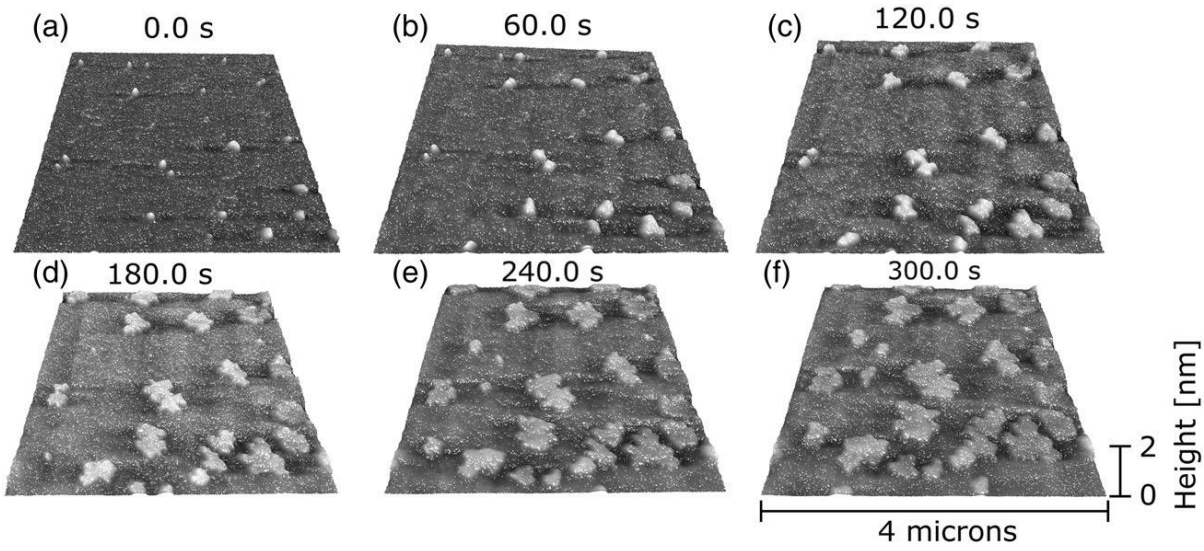

Figure 6 Selected frames form a Bristol contact mode HS-AFM video collected by Picco et al.[116] Each frame measures 4 × 4 µm in size with a pixel size of 4 nm, and was collected in 500 ms. The magnesium chloride crystals measure 1.2 nm in height. © [Payton]

Crystallisation of polyethylene oxide

Polymer crystallisation, especially in thin-film samples where surface effects can exert significant influence compared to bulk crystallisation behaviour, is very important because polymers are widely used as thin-film layers and coatings for a range of commercial applications.[120,121] A HS-AFM (VideoAFM™[122]) was used to directly measure several rapidly occurring polymer crystallisation processes. [123] The use of HS-AFM provided a real-space technique (rather than modelling or bulk measurements over many events) that could unambiguously measure key events, such as nucleation and crystal growth, directly. This application generated data that was used to confirm the validity of particular growth models.[124–126]

This is the first study where high growth rates can be observed with high spatial and temporal resolution (normally fast growth is measured with optical microscopy, which is inherently limited to low spatial resolution by the diffraction limit of light).

Corrosion of steel

The World Corrosion Organisation states that the current cost of dealing with corrosion globally is over 3% of the worlds GDP at $2.2 trillion annually.[127] Despite this large value, knowledge of the fundamental underlying processes is missing for many systems. Although the chemical processes may be well understood the time resolved process by which corrosion initiates and develops at the nanoscale in certain systems is not.[128] This is due to the environments in which corrosion typically occurs. In order to observe corrosion in real time, the sample must be mapped in a controlled gaseous or liquid environment. This prevents SEMs from being used to gain time resolved images of corrosion. HS-AFM has the temporal and spatial resolution and is able to image samples within in vivo conditions. Directly observing surface corrosion processes via HS-AFM is a challenging objective. When the corrosion occurs in a liquid environment gasses can be produced that can easily damage the delicate cantilevers or shield the sample under a bubble (see Fig. 7). When using any AFM, nano- and micro-sized gas bubbles have such high pressures inside that they appear almost solid to the AFM probe.[129] Figure 7 shows an optical view of an AFM attempting to image a pit forming in type 316 steel. Despite the bubbles attached to the spare cantilevers on the same chip, the tip of the currently used cantilever with the detection laser at its tip is still able to image the surface. However, the pit which is forming is shielded by bubble formation. Video rate data can be collected if the rate of gas production can be kept below the gas dissolution rate in the liquid. This can be achieved using a flow through liquid cell.

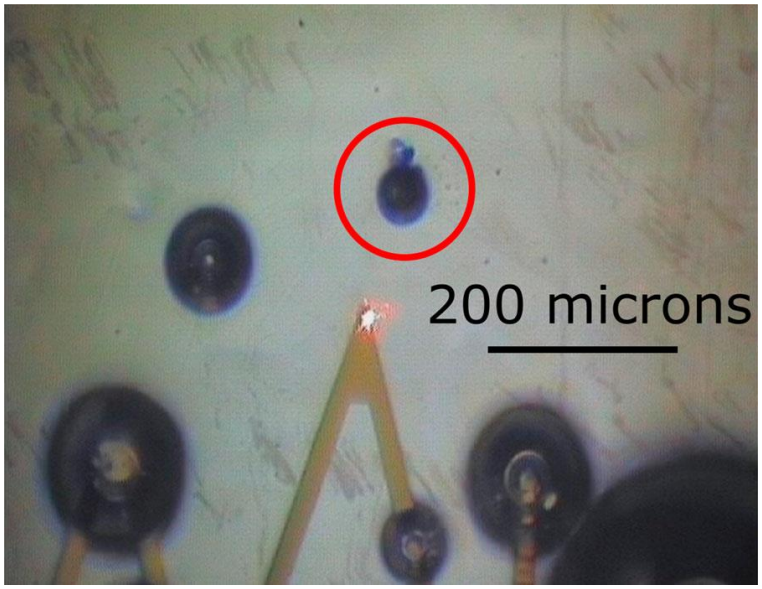

Figure 7 Optical image taken through an AFM showing bubbles effervescing from a corrosion pit (highlighted) in type 316 steel. Multiple bubbles have become attached to the spare cantilever's tips. The currently used cantilever with the detection laser at its tip (centre of the image) is still able to image despite the bubble attached to one of the cantilever legs. © [Payton]

The following example of observing nanoscale corrosion carried out by Laferrere et al. demonstrates the use of the Bristol contact mode HS-AFM to observe and better understand stress corrosion cracking in thermally sensitised type 316 steel.[130] The role of carbides in corrosion initiation is not fully understood and an experiment was designed to record the first stages of corrosion involving carbides at grain boundaries within a chloride environment.

Corrosion was simultaneously monitored and driven using a potentiostat to polarise the sample[131] and record the electrochemistry of the system using a three electrode fluid cell.[132] It is possible to use the cantilever itself as an electrode[133] however in the example shown the surface formed one electrode and the remaining two are suspended close to the cantilever in the chloride solution. Figure 8 shows two frames from the HS-AFM video that was taken during the experiment, showing carbide dropout. Images were taken every 500 ms and a grain boundary was located and observed during the polarising of the surface and the corrosion that followed.

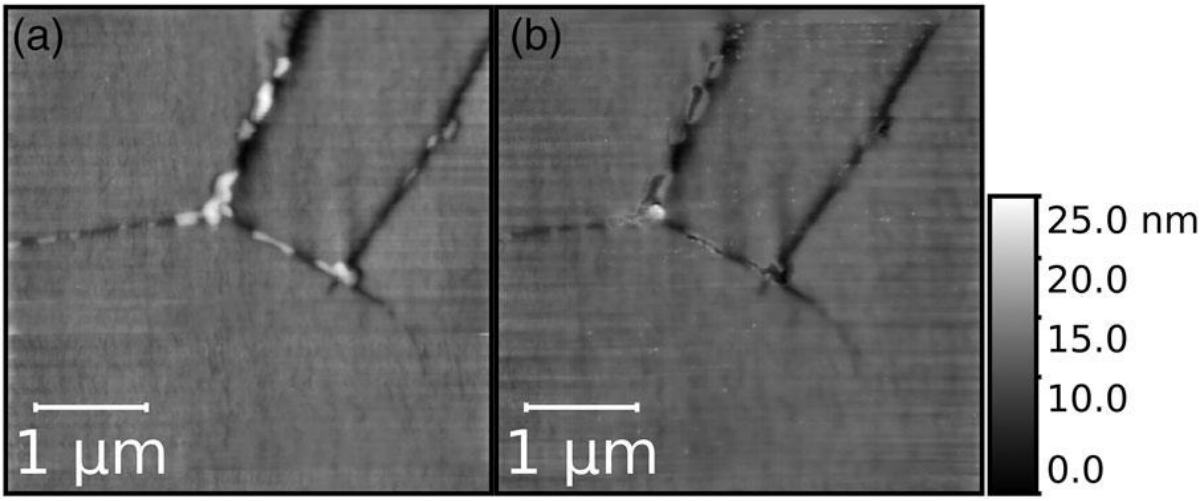

Figure 8 Two selected frames from the Bristol contact mode HS-AFM showing pre and post carbide drop out in a type 316 steel sample collected by Laferrere et al.[130] Each frame measures 4.3×4.3 µm in size and took 500 ms to collect with a pixel size of 4.3 nm

The successful outcome of this study has demonstrated the clear capability of HS-AFM to augment existing corrosion observation technologies, such as electro-chemical cells, to provide new insights into corrosion behaviour at the nano scale.

Summary

The HS-AFM allows dynamic events to be imaged at the nano and micro scale in controlled environments. The operation of HS-AFMs is also made more intuitive by being able to rapidly adjust the imaging settings and by instantly seeing the resulting image.[134] Similarly, video rate HS-AFMs are typically able to change the size of the imaging window such that the user can zoom into a section of the sample to view a feature in more detail. In this way, the operation of the AFM is becoming more like that of the SEM or optical microscope.

Large area, high-resolution surface characterisation

There are many situations within material science where macro sized areas require imaging with nanometre resolution[85,135–138]; these can fall under three main areas. The first is that a large image is needed to map the distribution of nanostructures over a large area. The second is that a greater area is required to be imaged in order to gather better sample statistics. The third is when the operator is interested in locating a rare nanoscale structure, or confirming that such structures are not present on a sample. All three are responses to the fact that at the nanoscale very few samples are homogenous. Most current analysis techniques map a small area and assume that the area to be representative of the whole surface which is often not the case, e.g. Lui et al.[139] Multi-beam SEMs[140,141] have been developed which can collect gigapixels per second using up to 91 parallel beams.[142] These tools can cover similar areas to HS-AFMs, however they have the same disadvantages as traditional SEMs when it comes to resolution and imaging environments.

Instead of collecting a video of a surface, the high pixel rate of HS-AFM can be used to image large areas with the same exceptional resolution AFM is known for. There are many ways that a HS-AFM can map large areas, from using arrays of AFM probes operating in parallel to offsetting the image area and tiling sequential HS-AFM images together. The following sections detail, through specific examples, work done to date in this area.

Imaging large structures

In the early 2000s, IBM developed what was hoped to be the next generation of data storage devices. The ‘Millipede’[143,144] was a technology based on a parallel array of AFMs. It used array of 1024 AFM probes to achieve a thousand-fold increase in read-write rates. Each probe could be actuated independently in Z to produce 1024 images in one motion of the imaging head (typically scanning at 10 Hz over a 92 μm range). Each of the probes was fitted with a thermal tip capable of writing structures in a thin polymer layer by locally melting the surface to write a bit on the surface. Ultimately, the technology was beaten in terms of data density by flash drives and the development of higher density magnetic disks. Although the most famous of the parallel HS-AFMs, the Millipede project is by no means the only version of this type, nor the first. In 1998, Minne et al. made use of up to 50 cantilevers[60] in a line array, to take images a centimetre in size.[61] Using a 10 cantilever array Minne et al. demonstrated the production of a 2 × 2 mm composite image of an integrated circuit with a pixel size of 400 × 400 nm. Using a tip scan speed of 1 mm s^{-1}, it took half an hour to produce this 25 megapixel image from 400 images. While this pixel rate is high, the pixel size is not suitable for very high resolution imaging. With multiple cantilever systems, each cantilever can operate at conventional AFM rates using readily available scan stages and avoiding the complex or high-bandwidth components required by HS-AFMs. However, each probe requires a separate detection system and this rapidly increases the overall complexity of the detection system electronics. Since optical detection systems do not easily scale it is common to find that each probe is self-sensing. [61,145–147]

More recently Seong et al. and Somnath et al. have both made use of a parallel HS-AFM to create composite images hundreds of microns in size[145,148] (as shown in Fig. 9). The HS-AFM used to collect the image in Fig. 9 made use of a custom probe chip containing 30 probes sensitive to heat loss at their tips (which is proportional to the distance between the tip and the surface) to plot the presented image.

Figure 9 Composite HS-AFM image collected by Seong et al.[145] using a custom cantilever chip consisting of 30 heat sensitive *cantilevers in parallel*

There are however drawbacks to multi-probe AFMs. Although they are capable of collecting large amounts of data in a short time, they require custom cantilevers that can be expensive as the technique has not yet become as main-stream as single cantilever methods. Due to the plate or line nature of the cantilever arrays used in parallel AFMs and the limited vertical range of each cantilever, parallel probe HS-AFMs have found their niche in imaging and writing nanostructures to very flat surfaces free of any sample slope.

Looking for rare features

It is important for quality control to know if structures are present on a surface, or indeed not present on a surface. Silicon fabrication often requires nanometre resolution over millimetre sized areas in order to assess masks for errors or for quality control during silicon integrated circuit production.[149,150] Indeed AFM calibration samples are often manufactured using the same silicon fabrication techniques used for integrated circuits.[151] If a large area piezo stage is being used, such as the one used on Ando's or Braunsmann HS-AFM[45,101] or a large area voice coil scanner such as the one used by Klapetek et al.[152] and Barnard et al.,[153,154] then a larger area (typically tens of microns to millimetres across) may be imaged as a single data set using a conventional raster scan. The use of voice coils to replace piezos as a means to achieving greater scan sizes can be traced back to Cantú et al. in 1987, where they were first used on a scanning tunnelling microscope,[155] and by Mariani et al. in 1998 on AFMs.[154,156]

When looking at low mass samples, voice coils offer a very attractive alternative to the more commonly used piezos. While they are not capable of providing the high forces and mechanical stiffness necessary to achieve fast scan rates in excess of 1 kHz, they are capable of far larger motions (millimetres or larger) without the high voltage supplies required by piezo-driven systems. Although the use of voice coil scan stages lowers the achievable scan frequency, the tip is still able to cover similar integrated distances to piezo systems at speeds over 1 mm s^{-1}. There are important considerations to take into account when using this approach, such as the thermal drift in the process of a single line scan. It is therefore typically necessary to run these large area stages in a closed loop fashion with metrological sensors constantly monitoring and correcting the position of the stage as it moves.[157–159]

As the length-scales of manufacturing techniques decreases, the need to carry out quality control over the processes will require tools with higher resolution and greater range than is available with the AFMs currently used. The authors expect HS-AFM to be a technology that will compete to fill this requirement in areas such as nanoparticle

characterisation[160,161] where the presence of rare, low concentration features must be found rapidly. Another example may be in the situation where a sample, such as a lithographic mask, may be damaged at the nanoscale and must be assessed. Such damage could be caused by radiation[162] or crystal defects[163] and would otherwise be very hard to map using an SEM or AFM.

The strength of HS-AFM to find rare nanostructures comes from the tools capability to image large areas without the drop in resolution associated with standard AFMs attempting to image ~100 µm sized areas. Typically HS-AFM have a preprogramed search pattern, usually a raster scan, which is usually hardware defined in the case where parallel cantilevers are used. However if a smaller HS-AFM window is translated about the surface then it would be possible to intelligently control the search for features of interest or follow nanostructures across the sample surface.[112]

Better sample statistics

It is possible to construct a large area map by moving the HS-AFM fast scan stage and combine the resulting images using custom software[78,113,164–167] to generate a composite HS-AFM image. This has several advantages as the user is able to observe the local imaging of the sample as the surface is translated under the cantilever tip allowing the quality of data to be assessed in realtime. [133] Using this method, the lateral pixel size of the image is now no longer affected by the size of the large area being mapped as there is no limit on the number of pixels in the final image, provided a computer can reconstruct the image. A single probe and detection system can map the whole area. This is particularly good for gathering sample statistics of nanostructures since results would not need to be calibrated from one tip to another as in a parallel HS-AFM setup.

With the piezo flexure stage mounted on top of a crossed pair of piezo stiction drive stages[111,168] the Bristol contact mode HS-AFM is able to map centimetre sized areas. The data from each frame can either be processed in real-time, to extract the important measurements (e.g. particle size distribution) and the image then discarded, or the final image can be constructed and then analysed. Software can be written to process and analyse the image in order to identify and count the number, location, or properties of specific structures. The data can then be presented in a way that describes the nano features of interest without the full (often multi-gigabyte) image having to be displayed.

An example of this application and the capability to analyse a large area and condense a full resolution image into a single plot is work done on characterising 2D materials by Howard et al.[169] In this situation, the HS-AFM is used to assess the quality, surface area and yield of exfoliated titanium disulphide monolayer sheets.

Figure 10 shows a section of a composite image collected using the Bristol contact mode HS-AFM and the measured monolayer thickness data plotted in a histogram. Software was written to measure the step height of each flake as described in Howard et al.[169] From these measurements the mean thickness was measured as 1.067 nm. The advantage of this technique is that a far larger area on the surface can be analysed when compared to conventional AFM, thus allowing orders of magnitude more flakes to be characterised.[170–172] HS-AFM brings with it the power to reach a statistically valid measurement without requiring the user to determine a representative region (which is often a very subjective process) of the sample for a publication.

In order to build a composite image of the sometime tens of thousands of individual HS-AFM frames, it is important to understand the sources of error in the linearization of each frame[77,78,152] and to correct for this.[78,173] This can be carried out using metrological sensors[77] on the fast and slow axis proving traceability for any errors or in software using a feed-forward control on the waveform generation for the two axis.[74]

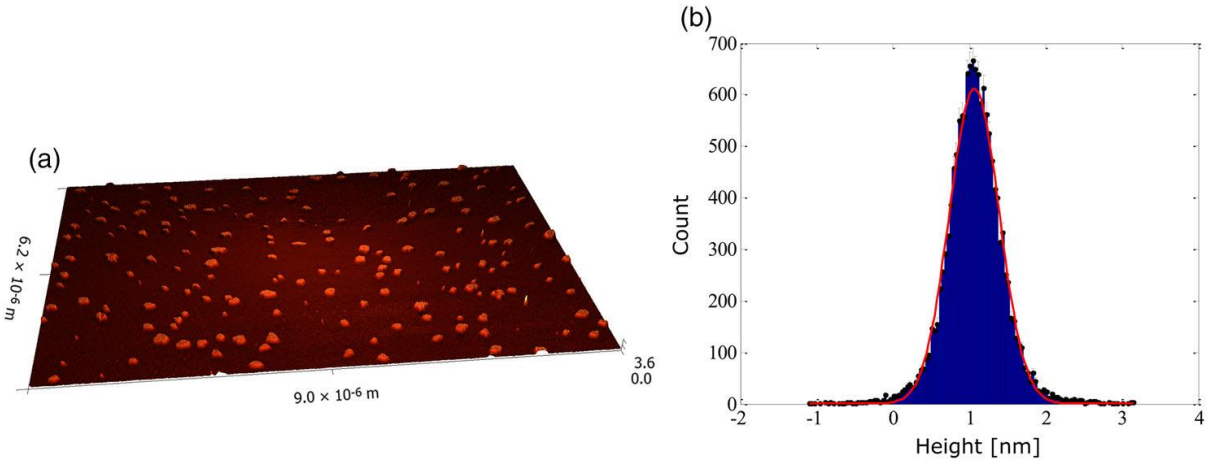

Figure 10 a HS-AFM composite image of TiS_2 flakes only 1 lattice space thick on a mica substrate. The image was collected using the Bristol contact mode HS-AFM and is a small section of a much larger dataset. b Histogram of step heights as measured using an automated process as described in Howard et al.[169] The mean lattice thickness was measured to be 1.067 nm.

Summary

It is the authors opinion that single probe HS-AFM have greater versatility and flexibility compared to multi-probe HS-AFMs for applications to large area mapping. In particular, the fact that a single probe HS-AFM provides a very responsive, video-rate image of the sample surface (rather than slowly compiling an image over tens or hundreds of seconds) enables the user to rapidly respond to changes in tip quality (through contamination or tip wear) and to rapidly respond to any issues with sample quality or instrument function.

Mapping material properties other than topography

Since the probe tip is in physical contact with the surface, it is capable of measuring the material properties of the sample at the nanoscale, often in a non-destructive manner. Such modes enable AFMs to map: topography as has been shown previously, friction,[23,26,174] adhesion,[175–177] or nano-mechanical properties such as local stiffness, [40,178–185] electrical[186,187] and thermal[143,188] conductivities. The following sections detail the use of a HS-AFM to map material properties. These techniques could be used to either observe a change in the property being measured with time as a video or to map the property over large areas, often simultaneously with the sample topography.

Hardness

It is often important to identify nanostructures within a bulk material as these nanostructures can affect the mechanics of the bulk material.[191,194] An example of this is in type 316 steel commonly used in high value plant components. Inclusions within steels such as carbides or sulphides, if not dispersed evenly throughout the bulk, may locally affect the material strength,[195] ductility[196] or hardness[196,197] possibly to the extent that the properties of the steel are no longer within designed tolerances.

As an essential component in steel, the distribution of carbon at the nano and microscale affects the local properties of the bulk material. An increased concentration in the form of carbides increases the hardness of the steel but also how brittle the steel is.[198] SEM elemental mapping techniques such as energy dispersive x-ray (EDX) are traditionally very poor at characterising the quantity of carbon present on the sample due to surface contamination by the electron beam depositing material on the surface during imaging.[199]

HS-AFMs have been used to assess the distribution of carbides within type 316 steels.[189] The process relies on the specific sample preparation steps to enable the HS-AFM to map carbides due to their increased hardness.[190] By mechanically polishing the sample, harder regions remain proud of the surface while softer regions are polished away leaving lower structures in the topography map. This hardness induced topography is of the order of nanometres (as shown in Figs. 11 and 12c) with the topography being proportional to the hardness of the local area on the surface. Due to the sample preparation the process is not able to give a quantitative hardness measurement, instead a relative hardness map is produced.

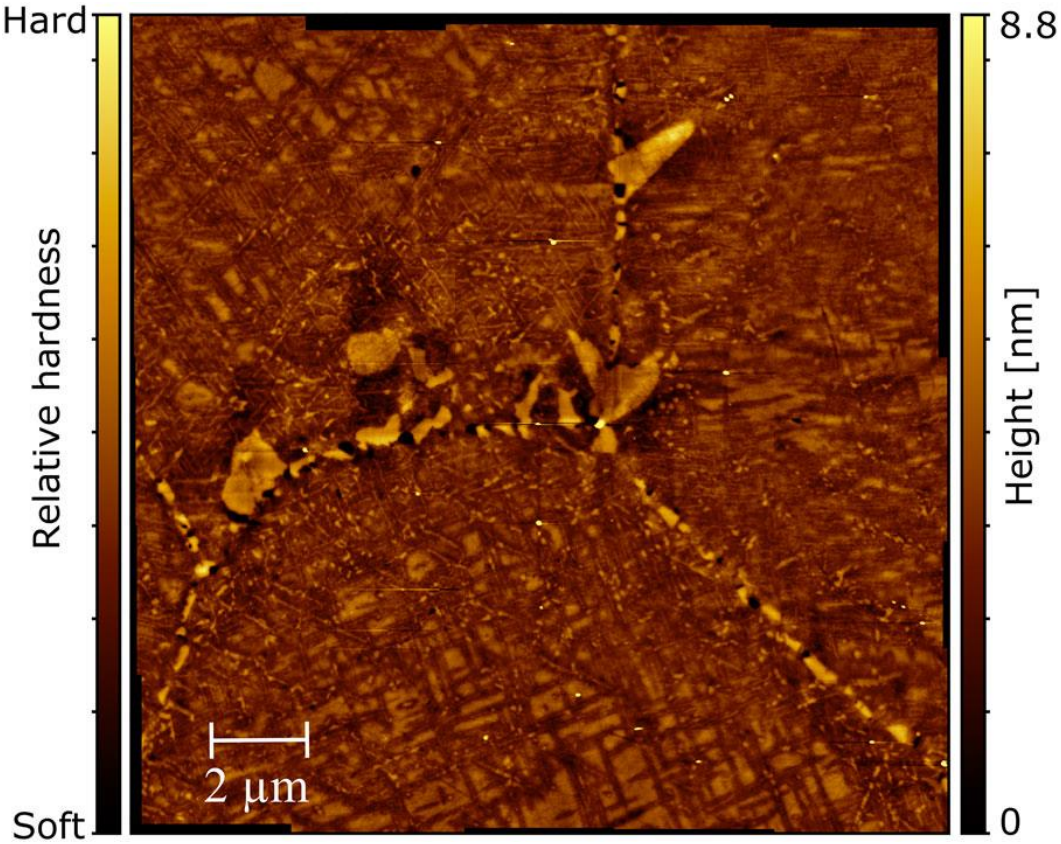

Figure 11 Composite HS-AFM hardness map. Collected using the Bristol contact mode HS-AFM by Martinez-Ubeda et al.[189] The sample was mechanically polished following the protocol outlined in Warren et al.[190] Data were collected at 2 megapixels per second and a frame rate of 2 fps with a pixel size of 3 nm. The 27 megapixel map was collected in 50 s.

This method is able to map grain boundaries, twins, inclusions, carbides and cavities clearly right down to the nanoscale.[189] Figure 11 shows hardness induced topography over a 240 μm^2 area of type 361 steel prepared following the instructions outlined by Warren et al.[190] The composite map was collected using a contact mode HS-AFM at 2 megapixels per second with a pixel size of 3 × 3 nm and 500 ms per frame. The whole 27 megapixel hardness map was collected in 50 s.

It was found that a steel sample exposed to high pressure, temperature, and high carbon environment forms nano- and micro-sized carbide structures that are particularly hard to map using existing techniques due to their size. Using the sample preparation described previously these carbides can be mapped using the same contact mode HS-AFM used to collect the data shown in Fig. 11.

Figure 12b shows an example of a large area composite image (~10 000 μm^2) mapped using the Bristol contact mode HS-AFM of a type 316 steel which has been prepared as described previously. The image is over 600 megapixels in size with a pixel size of 4 × 4 nm and took under 20 minutes to collect. A corresponding SEM image is also shown in Fig. 12a for comparison. While the SEM successfully maps the grain orientation which is apparent as light or dark grey areas, it does not have the resolution necessary to image the nanostructures present in the sample topography as shown in Fig. 12c, which is a full resolution frame from the HS-AFM Fig. 12b as indicated.

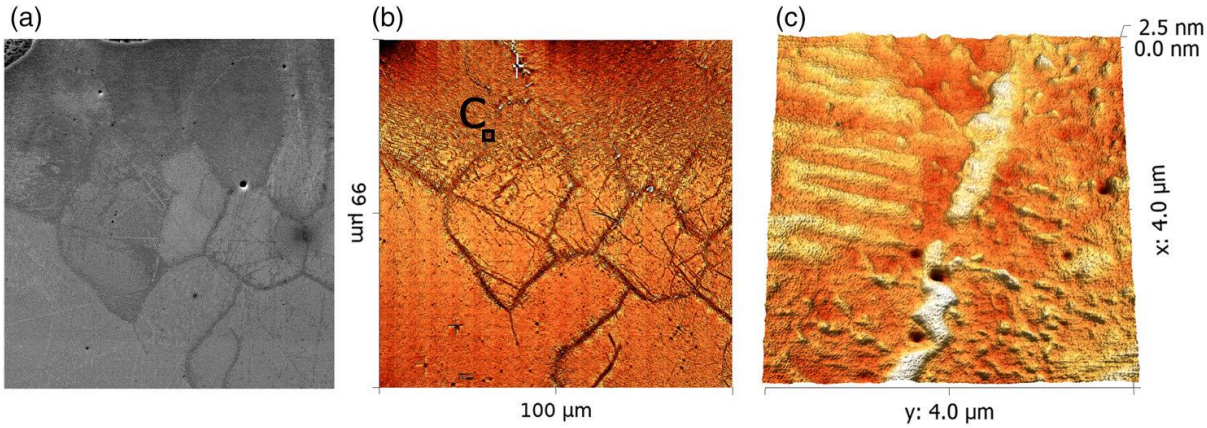

Figure 12 Comparison of HS-AFM to SEM while imaging the same 100 × 98 µm area of type 316 steel. The sample has been mechanically polished in order to show the hardness in the topography. a The SEM image to the same scale as the Bristol contact mode HS-AFM composite image shown in b. c A zoom onto a single HS-AFM frame on a grain boundary at the location *shown in b. © [Payton]*

To date the best way of viewing these carbides has been to use a focussed ion beam to prepare a cross section for a transmission electron microscope (TEM),[200] or to chemically etch the polished sample surface and observe the resulting pattern using an SEM,[201] or to use a standard AFM.[202] These methods all have limitations; the TEM has a significant resolution advantage over SEM but is only capable of imaging a small sample area. The SEM is not capable of observing the smaller carbides such as those within the grain boundary of the metal. AFM, like TEM is just too slow to allow statistically valid areas to be mapped. HS-AFM has the benefits from both the SEM and TEM when characterising carbides.

The ability of HS-AFM to measure hardness in a repeatable fashion over the same sample area (unlike nanoindentation) [203] means that hardness mapping could be carried out as part of an existing sample characterisation workflow. The downside of using this technique is that it will only provide a relative measurement of hardness, as the absolute relationship between hardness and topography will rely heavily on the type and duration of the polishing during the sample preparation. Common sense must be used in the interpretation of hardness induced topography maps as polishing artefacts such as scratches and the removal of loose surface features can be present on the surface. Following the protocols set out by Warren et al.[190] will minimise the presence of artefacts.

With the 'Big Data' that HS-AFMs can produce, software has been designed[204] to map out typical features found across many materials. Using this software, the huge amount of data collected during a HS-AFM large area map can be condensed down to answer the questions posed by the operator.

This software has been used to great strength when assessing the carburisation of steel components in samples similar to those described above.[204] Figure 13 shows it is possible to measure thousands of carbides across hundreds of microns and map their distribution. These values can be placed into computer models[205–207] and used to predict how a growth in density of carbides can affect the strength of type 316 steels with time. The software uses a local threshold to identify features with positive relief. In the future more advanced machine vision and learning processes could be incorporated to better distinguish signal from noise.[208]

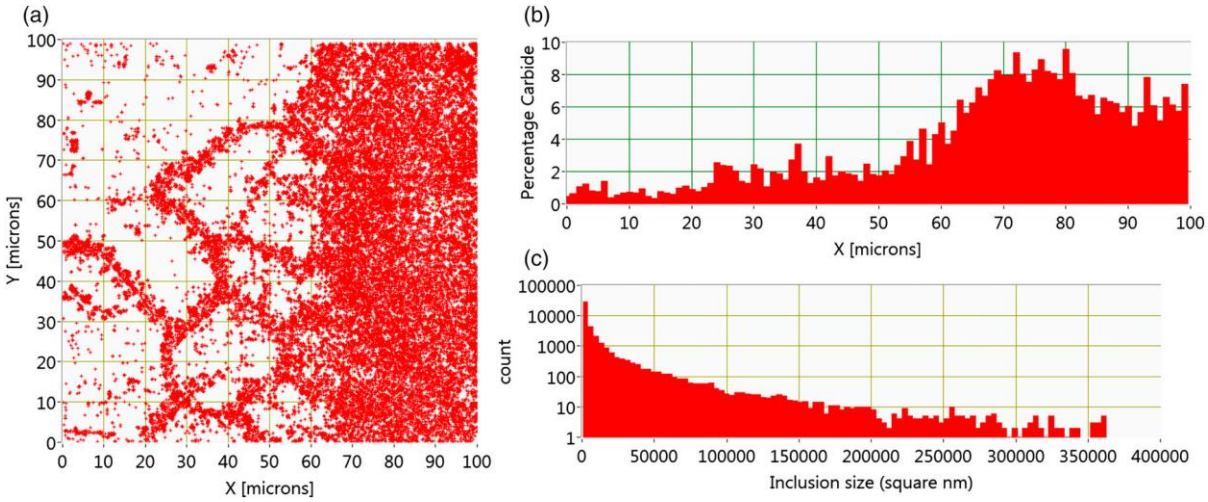

Figure 13 Three plots of the example data that can be extracted from a large area HS-AFM map, in this case the map shown in Fig. 12b has been processed to extract data about the number and density of inclusions (carbides). a The coordinates of the carbides on the sample, b shows a histogram of the percentage of the sample containing carbides in from the edge of the steel (at 100 µm), and c shows a histogram of the carbide size in nm^2. In this heavily carburised area 41 730 carbides were mapped. © [Payton]

Mapping stiffness variations with contact resonance force microscopy

Using a technique called contact resonance force microscopy (CR-FM)[209–211] coupled with a contact mode HS-AFM it is possible to measure the relative stiffness of a sample simultaneously with the samples topography at each pixel.

CR-FM measures the stiffness of the sample by observing the frequency shift of a deflection mode resonance peak of the probe as the tip moves from one material to another.[95,182,210,212] Figure 14a shows the schematic of a CR-FM system. By assuming that the properties of the cantilever remain constant, any frequency shift in the coupled cantilever–local sample system is assumed to be due to changes in the local sample stiffness. The reference signal from the lock-in amplifier is used to excite the cantilever[185] of the HS-AFM at a frequency located on the downward slope of a resonance peak of the cantilever that has a stiffness associated with it that is similar to the stiffness of the surface being observed, as shown in Fig. 14b. The user selects a specific peak by carrying out a frequency sweep of the lock-in frequency, until contrast is observed in the image. The CR-FM then infers a relative stiffness from an observed frequency shift[178,209]; the stiffer the local sample the higher the resonance frequency of the system. With knowledge of the cantilever properties, it is possible to calibrate the CR-FM signal into a Young's modulus value of the local sample under the cantilever tip.[178]

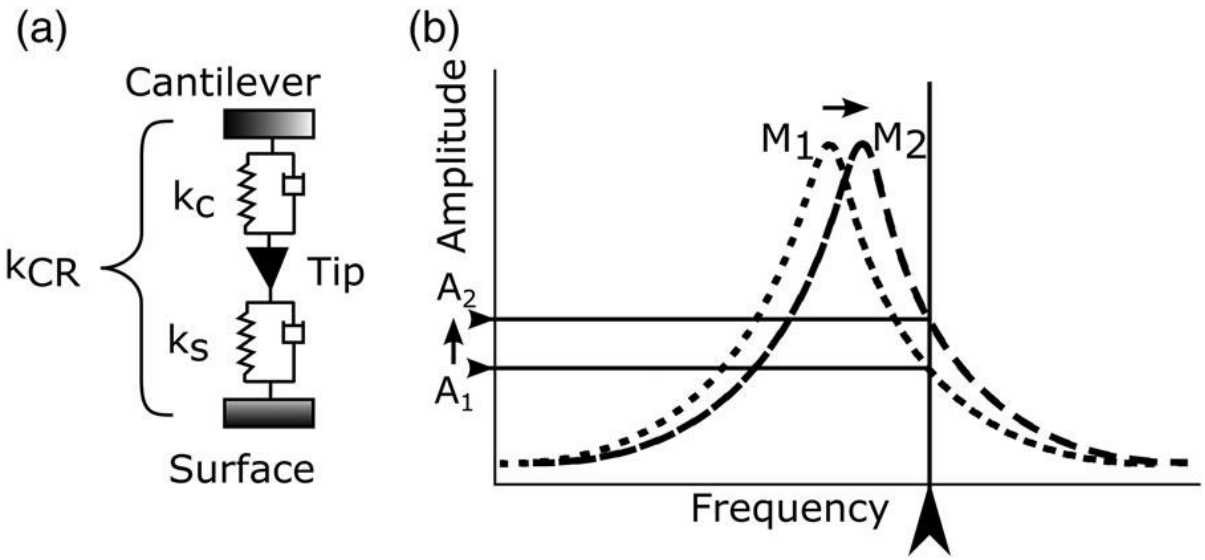

Figure 14 a Schematic model of the contact resonance method. The local surface under the tip has stiffness k_s and the cantilever mode has stiffness k_c, the combined stiffness k_{CR} of the local sample–cantilever system is measured by observing shifts in the resonance frequency of the system, as k_c is assumed constant, k_s can be inferred. b A schematic of a plot of lock-in amplifier amplitude against frequency. The dotted line shows the position and shape of the resonance peak material 1 (M_1) and the dashed is the resonance curve for when the tip is on material 2 (M_2). The curve for M_2 has a peak at a higher frequency than M_1 signifying that M_2 is stiffer than M_1. In this

form of Contact Resonance the lock in frequency is maintained at the frequency marked with the arrow on the frequency axis. As the tip moves from material 1 to 2 the lock in amplifier signal increases from A_1 to A_2. © [Payton]

Standard CR-FM typically uses the fundamental resonance of the system,[209] however there are two very important benefits of using higher modes in the system[210]; first a soft fundamental mode allows for lower forces to be imparted into the sample, thus the sample is at less risk of damage; and second the higher frequency associated with the higher mode of the cantilever allows for a faster time constant in the lock-in amplifier and hence more measurements of stiffness to be made per second. The down side of using higher modes is that the errors involved with calibrating the higher modes can be as high as 60% in the second eigenmode[213] and progressivelyworse with mode number. The technique make use of a thermal spectra of the cantilever's motion which potentially limits the maximum mode used due to the signal to noise ratio of the detection system. Therefore data collected using a higher mode number such as the data in Fig. 15 often just show a relative contact resonance amplitude.

Figure 15 shows example data of high-speed CR-FMcollected using the Bristol contact mode HS-AFM by Payton et al.[189] The composite contact resonance map shown in Fig. 15 shows islands of titanium evaporated onto a silicon substrate. To show that multiple materials can be identified collagen fibres have also been laid across the sample surface. In Fig. 15, the HS-AFM height data is used to create the 3d image and the simultaneously collected CR-FM data was used to provide the colour scale. In this figure, the stiff silicon surface is strongly differentiated from the softer evaporated titanium islands and the deposited collagen fibres. The technique has been shown to have excellent spatial resolution as the contact resonance frequency shift occurs instantly as the tip moves from one material to another.

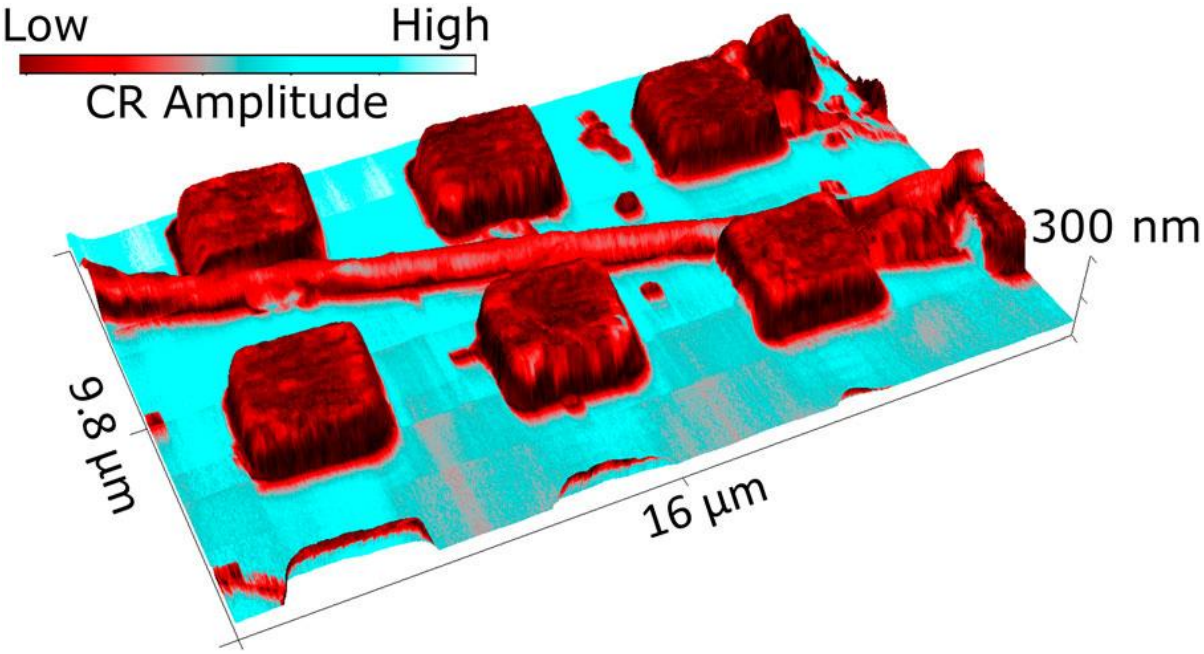

Figure 15 Composite CR-FM map of a 16 × 9.8 µm area of titanium (110–125 GPa[214]) patterned silicon substrate (165 GPa[214]) with a collagen fibre (1–10 GPa[214]) deposited diagonally across. The titanium, which is softer than the silicon has far lower contact resonance amplitude compared to the silicon. The contact resonance signal has been placed as a texture over the sample topography which was simultaneously collected. The 13.5 megapixel map was collected in under 30 s by Payton and Picco et al. using the Bristol contact mode HS-AFM[189]

It is expected that with further work on the calibration of the stiffness of higher deflection modes in AFM probes, CR-FM will overtake nano-indentation[215–217] as the preferred method for mapping out stiffness variations across a surface. CR-FM is capable of mapping out a relative stiffness in a non-destructive,[218] repeatable fashion with tip convoluted resolution. When compared with nano-indentation, CR-FM becomes an attractive alternative given the destructive nature of nano-indentation and the reduced resolution of the technique due to the stress field induced in the sample by the indent.[217] While there are alternative methods to CR-FM for mapping the local Youngs Modulus, such as Peak Force AFM these require a force curve for each pixel coordinate. [219] The fastest to date making use of small cantilevers only 10 µm long has demonstrated the capability to collect 300 pixels per second,[219] however it is unlikely that the pixel rate will increase much beyond this value do to the difficulty in using such small cantilevers in practice.

Piezo-response force microscopy

The piezo-response response of a ferroelectric thin films[220,222] can be mapped at high speed using a technique called high-speed piezo force microscopy (HSPFM)[223] developed by Nath et al. The technique allows the observation of domain nucleation and growth in ferroelectric materials. An AC bias voltage is placed between the ferroelectric material sample and a conductive probe. The bias causes a piezoelectric effect within the ferroelectric material which causes a displacement to be measured by the HSPFM probe. The frequency of the electrical AC signal is chosen to be near a contact resonance peak to enable a mechanical amplification of the signal. A lock in amplifier measures the phase of the probes mechanical response to the AC electrical signal. Nath et al.[223] use the phase to map the domain orientation sample directly under the tip with a lateral resolution of 5 nm. A 'stroboscopic technique' was used to allow the domain orientation flipping to be recorded at each pixel with 49 µs temporal resolution. Due to the flatness of the sample (sub-nanometre rms roughness) the control loop was disengaged on a commercial AFM (Asylum Research MFP- 3d-SA) which allowed a frame rate of six frames per second (128 by 128 pixels). Such experimental setups allow the dynamics of domain flipping and grown to be observed.

Coefficient of friction

The capability of HS-AFMs to repeatedly image the same area at high frame rates allows the tool to carry out parameter sweeps of the physical properties of the sample in a fraction of the time compared to a conventional AFM.[26,221,224] Bosse et al. varied the load the cantilever places on the surface in each frame while measuring the difference between the maximum and minimum tortional signal from a contact mode HS-AFM.[76] The resulting data allows the coefficient of friction of a material to be plotted at the nanoscale. Figure 16 shows a coeffiecient of friction map collected by Bosse et al. The surface contains silicon dioxide and a round exposed gold region.

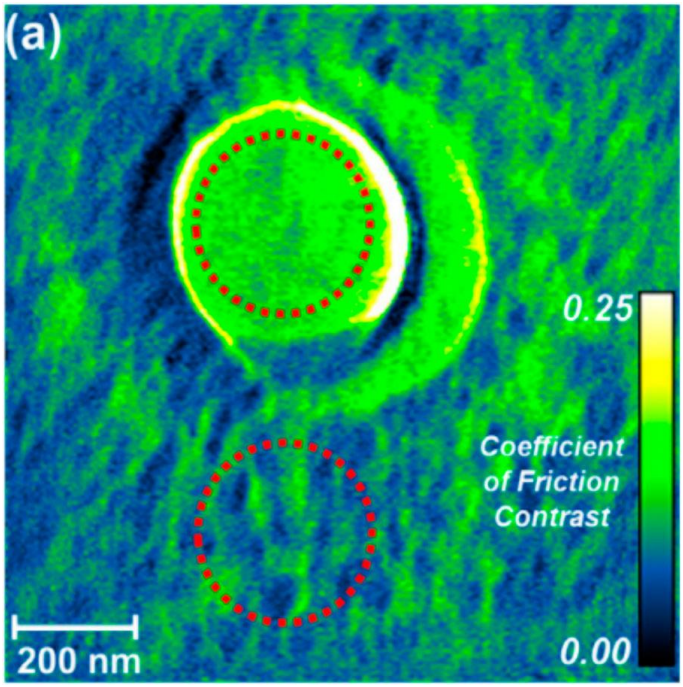

Figure 16 Data from Bosse et al.[23] by varying the load on the surface and observing the torsional motion of the cantilever the coefficient of friction can be mapped at the nanoscale. The figure shows the contrast between a substrate of SiO_2 and an exposed circle of Au.

Atomic resolution of stick-slip events

By using small range piezos in their flexure based parallel-kinematic sample scanner Braunsmann et al. have demonstrated the ability to show atomic resolution in the form of the stick-slip effect on muscovite mica {001} cleavage plane at 3 frames per second over a 2.8 × 2.8 nm image Fig. 17.[45] Although the topography of the atomic lattice of the mica is presented only in the stick-slip of the cantilever passing over the surface, the resulting pattern matches the expected hexagonally arranged SiO_4 and AlO_4 tetrahedrons. The demonstrations of atomic and molecular resolution using HS-AFM are a testament to the extreme precision, accuracy and control of the tip-surface interaction forces possible even at pixel rates of 0.5 megapixels per second.

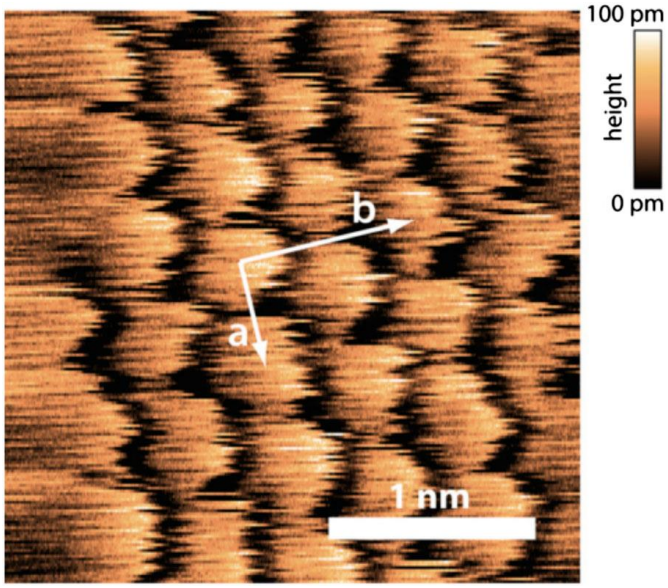

Figure 17 Selected frame from a HS-AFM video recorded at 3 frames per second collected and published by Braunsmann and Schäffer.[45] The data display atomic stick slip on a muscovite mica {001} cleavage plane

Summary

As HS-AFM technology develops further, AFM measurement techniques will be translated and integrated into the HS-AFM suite of capabilities. Currently, the main limiting factor for the collection and mapping of quantitative material property values is the lack of reliable methods for the calibration of the cantilever probes used. Although there are existing techniques for the calibration of the fundamental bending mode,[225,226] many of the mapping techniques require knowledge of the stiffness of the probe's higher bending and tensional modes. Work is being carried out in a number of laboratories around the world[210,213,227,228] to calibrate the properties of these modes.

Fabrication of nanostructures

It has been demonstrated that HS-AFMs can be used to aid material science by observing and mapping samples. However, this is by no means the limit of the tool, the high sample throughput and resolution, coupled with the physical nature of the imaging tip, means that the HS-AFM can also be used to mark, pattern and print on material surfaces. AFMs and HS-AFMs are capable of writing these structures to surfaces,[52,143,145,167,229–244] in a technique called nanolithography. As with many of the imaging modes, the methods described here have been transferred from standard AFMs. The ability for HS-AFMs to write nano and micro-structures to surfaces enables larger areas to be covered compared to standard AFMs. As with the variety of imaging modes available to HS-AFM, there are numerous nanolithography modes which have been used on HS-AFMs. The following section explains the different modes of HS-AFM nanolithography.

Local oxidation-based nanolithography

Nanostructures can be written to surfaces using localised oxidation[167,229,236,238–241,245,246] of the substrate. This is the earliest form of AFM-based nanolithography[247] and, as shown in Fig. 18, structures are written to the surface by applying a bias between a conductive surface and a conductive cantilever. The sharp tip of the probe concentrates the electric field, creating oxyanions within the fluid meniscus, which locally oxidises the surface under the tip. In the case of a silicon[240,246,248] the silicon oxide produced is less dense and so stands proud of the surface as a structure.

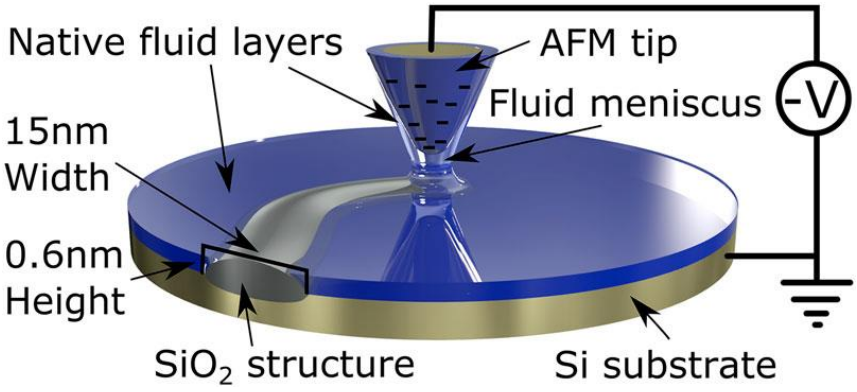

Figure 18 Schematic of a conductive AFM cantilever performing local oxidation of a silicon substrate in order to write nanostructures to the surface. By placing a potential between the tip and the surface oxyanions are produced which react with the silicon surface to build oxide structures which are less dense than the standard substrate and so stand proud of the surface. © [Payton]

The size of the structure is dependent on the number of oxyanions produced. This number is proportional to the amount of time the tip is at any given location and the bias voltage between the tip and surface as described by Vicary et al.[241] By pulsing the tip bias on at the same location in the frame as a HS-AFM scans, a surface structure can be written in real-time. The process depends on the ambient fluid layers on the sample and tip. It is therefore important for the humidity and temperature of the imaging environment to be controlled during the writing process. The aspect ratio of these structures can be further enhanced using plasma etching after the initial structures have been written.[248] The structures shown in Fig. 19 were written to the silicon substrate using the Bristol contact mode HS-AFM using a tip bias of −10 V. The same oxidation nanolithography has been used on HS-AFMs making use of multiple cantilevers to parallelise the process across macro sized areas.[167]

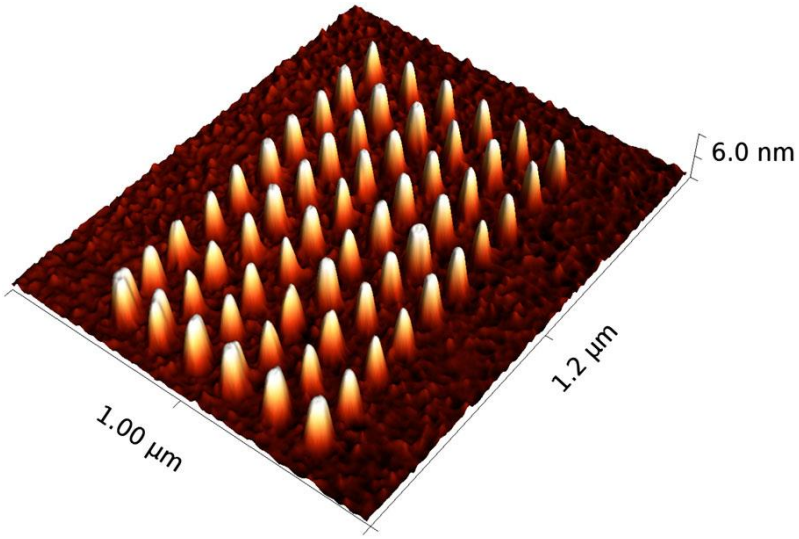

Figure 19 Contact mode AFM image of nanostructure written to the silicon substrate using the Bristol contact mode HS-AFM.

Thermally driven modifications

Nanostructures can be written to surfaces using heated probe tips. Due to the small thermal mass of the tip, temperature gradients of 1000°C μs^{-1} can be achieved.[146] This allows structures to be melted into a polymer substrate even when the tip is passing across the surface at speeds in excess of 20 mm s^{-1} [231] allowing high throughput of high aspect ratio nanostructures. Parallel HS-AFM systems can be equipped with thermal nanolithography capability[145] as shown by the original IBM Millipede system[143] and Illinois' heated micro cantilever array system. [148] IBM's Millipede made use of multiple (an array of 32 × 32) cantilevers in an attempt to use the process for data storage, achieving storage densities of 0.394 Gb cm^{-2}.[144] Each of the micro-cantilevers had an independent heating element at its tip capable of melting small areas of a polymer substrate to represent bits. Ultimately, the storage density of magnetic media and flash based ICs surpassed the densities achieved by the device, and work was discontinued. However, thermal tips can also be used to alter the chemistry of a surface, such as creating graphene oxide on surfaces of graphene[242,249] or writing graphene structures by thermally reducing graphene fluoride,[243] which provide many new opportunities and application spaces for this technology.

Dip pen nanolithography

The previous two types of nanolithography are very well suited to HS-AFM, as the time to write a single pixel is fast. The Dip pen technique[232,233,250,251] is slower per written pixel, however, it allows a wide range of materials to be 'printed'.[251,252] The method flows a fluid of the material to be written to the nanostructures down the tip which is then placed onto the surface just like ink from a pen.[252] The technology has been converted into a high-speed nanolithography technique by using arrays of tens of thousands of tips to write thousands of structures simultaneously.[52,253,254]

Plowing

Plowing is a nanolithography method which uses the physical tip of the cantilever to mark the surface.[255–257] It has the advantage that almost any sample can be patterned however there is the increased risk of tip wear due to the increased load on the surface which the tip must exert.[258]

Summary

The use of HS-AFMs carrying out nanolithography will begin to play a greater role in material science, as significantly larger areas are now able to be altered and written to. It is envisaged that HS-AFM nanolithography will soon provide a similar level of usability and functionality than is provided by conventional 3D printers, to pattern surfaces with custom nano-structure textures. While currently the sample throughput is not up to industrial rates, it does have the ability to rapidly experiment with nanostructures on surfaces, possibly creating prototype functional material surfaces before up-scaling to conventional manufacturing processes. Nanolithography also has the possibility to succeed at small scale conventional IC manufacturing and product development processes, as it has a resolution that exceeds all the current mask based manufacturing methods[146] at a far lower cost and energy requirement.

Future of HS-AFM

While many imaging, mapping and lithography modes from standard AFMs have been incorporated into HS-AFMs, there are others that could greatly benefit the field of material science. Many of the current limitations on the image quality and speed of imaging are merely due to engineering challenges that can be overcome, however, some are due to the physical properties of the materials and sizes of the components used, this is most obvious in the cantilevers used. The current trend towards using small cantilevers to up the speed of intermittent contact HS-AFMs will reach a limit when it is no longer practical to align a laser onto the back of the cantilever and mount the cantilever within the HS-AFM. Although we may see a limit to the available speeds of HS-AFM there will be a push to gather more information from the sample while imaging. This section will outline briefly these methods.

Multimodal imaging

Although there are some exceptions,[66,90,91] the control loops of intermittent and non-contact AFMs and HS-AFMs require at least one full oscillation per pixel. As cantilever and detection technologies develop, it should be possible to measure the cantilever's response to surface forces at frequencies other than the driving frequency on an intermittent contact mode HS-AFM. This technique, known as multimodal AFM[259–261] is able to construct maps of multiple material properties simultaneously[259] across the sample on conventional AFMs. In order for higher modes to be observed in an intermittent contact HS-AFM, a very high-bandwidth detection system and an FPGA-based lock-in amplifier will be required to measure resonances in excess of 10 MHz.

Electrical properties

By using a conductive cantilever, such as one coated in platinum or gold it is possible to map the electrical properties of the sample[186,187,262–264] on a standard AFM. Currently the noise floor of the transimpedance amplifiers necessary to amplify the picoamp current flowing through the cantilever tip is too high to allow the megapixel sample rates required by HS-AFM. Non-contact electrical measurements such as electrostatic force microscopy (EFM)[265] could be used at high-speed by interleaving line scans in contact mode or intermittent contact mode then lifting a small distance from the surface to measure the electrostatic force between the surface and a conductive biased cantilever. The short time between height measurements and electrical measurements would minimise drift in the measurements but would also require a very accurate control loop to maintain the surface-tip separation. Research would also have to be undertaken in order to mitigate the excitation of the cantilever from the control loops response to rough surfaces.

Tip scanning

Due to the requirements of aligning a laser onto the back of most cantilevers used in HS-AFMs, the majority of HS-AFMs use a sample scanning method to build up the final image (as discussed previously). However this places limitations on the size and mass of the samples that can be imaged. A tip scanning AFM could instead be placed onto a static sample and hence any size of sample could be imaged. Some advances towards tip scanning HS-AFMs have been made[73,167] and it is expected that the ability to scan arbitrary large objects will drive the development of further tip scanning HS-AFMs.

Summary

The most likely developments of HS-AFM for use in material science over the coming years will be in the increased usability of the tool, as its acceptance in the field increases. The second most important development will be in the continuing drive for quantitative, not just qualitative, property maps. These have also been the key goals of conventional AFMs as they have developed over the last three decades.

There are situations within materials research where AFMs have been found to be the best tool to carry out characterisation[266] except for their sample throughput. It is expected that in time the uptake of HS-AFM technology will enable new standalone sample specific tools (for example a box that characterises nanoparticles) to become available that can rapidly carry out the characterisation of nanomaterials with no compromise in resolution. These tools will allow the material scientist new ways to assess failure mechanisms, new materials, coatings and processes. Key areas in which HS-AFM would be able to aid current material research challenges would be in the analysis of: nanoparticles (size and shape simultaneously), biomaterial research (in vivo mechanical maps), surface coatings (quality control), materials for energy storage (nano-pore measurements), smart martials (real-time observation of the materials response). This list is by no means exhaustive, the current limitation is in the number of HS-AFMs available to the materials research community, a fact that will hopefully be overcome in time.

Conclusion

Since their invention, AFM has moved far from its beginnings of mapping just sample topography and is now able to map a whole host of material properties. Very soon after its invention it became clear that its main limiting factor was the speed at which it operates, due to the hard work of many research groups globally the pixel rate of AFM has increased from 1 pixel per second in 1987[1] to tens of megapixels per second today.[67] This increased pixel rate can now provide either video rate imaging of dynamic events or images of macro sized surfaces with nanoscale resolution. HS-AFM is now becoming a tool that is of use to many different industries, not just academic research, especially in the field of material science. It is the author's opinion that HS-AFM is still very much in its infancy and that, just as the SEM has enabled huge academic and industrial leaps in material science, HS-AFM will soon follow suit and enable a greater understanding of materials at the nano and micro scale.

Acknowledgements

The authors wish to thank the Royal Academy of Engineering for supporting Dr Payton and Dr Picco.

References

[1] G. Binnig, C. F. Quate, and C. H. Gerber, "Atomic Force Microscope," *Phys. Rev. Lett.*, vol. 56, no. 9, pp. 930–933, Mar. 1986.

[2] S. Morita, "Atom world based on nano-forces: 25 years of atomic force microscopy," *J. Electron Microsc. (Tokyo).*, vol. 60, no. SUPPL. 1, pp. 199–211, 2011.

[3] "ZEISS Gemini SEM Family," *Product Information Version 2.0*, 2016. [Online]. Available: http://applications.zeiss.com/C125792900358A3F/0/8AA75F6A864B2BBAC1257E180037CCA0/$FILE/EN_40_011_095_GeminiSEM_rel_2_0.pdf. [Accessed: 01-Jan-2016].

[4] D. Batchelor and P. Russell, "SEM and AFM: Complementary Techniques for

Surface Investigations," *Microscopy and Analysis*, 2013. [Online]. Available: http://www.microscopy-analysis.com/magazine/issues/sem-and-afm-complementary-techniques-surface-investigations. [Accessed: 28-Jan-2016].
[5] A. Delvallée, N. Feltin, S. Ducourtieux, M. Trabelsi, and J. F. Hochepied, "Direct comparison of AFM and SEM measurements on the same set of nanoparticles," *Meas. Sci. Technol.*, vol. 26, no. 8, p. 085601, Aug. 2015.
[6] K. C. Grabar, K. R. Brown, C. D. Keating, S. J. Stranick, S. L. Tang, and M. J. Natan, "Nanoscale characterization of gold colloid monolayers: a comparison of four techniques.," *Anal. Chem.*, vol. 69, no. 3, pp. 471–477, Feb. 1997.
[7] J. E. Castle and P. A. Zhdan, "Characterization of surface topography by SEM and SFM: problems and solutions," *J. Phys. D. Appl. Phys.*, vol. 30, no. 5, pp. 722–740, Mar. 1997.
[8] X. C. Tong, *Advanced Materials for Thermal Management of Electronic Packaging*. Springer Science & Business Media, 2011.
[9] G. Binnig, H. Rohrer, C. Gerber, and E. Weibel, "Tunneling through a controllable vacuum gap," *Appl. Phys. Lett.*, vol. 40, no. 2, pp. 178–180, 1982.
[10] Editorial, "A brief history of some landmark papers," *Nat. Nanotechnol.*, vol. 5, no. 4, pp. 237–237, Apr. 2010.
[11] U. Dürig, D. W. Pohl, and F. Rohner, "Near-field optical-scanning microscopy," *J. Appl. Phys.*, vol. 59, no. 10, pp. 3318–3327, May 1986.
[12] P. Hansma, B. Drake, O. Marti, S. A. Gould, and C. B. Prater, "The scanning ion-conductance microscope," *Science (80-.).*, vol. 243, no. 4891, pp. 641–643, Feb. 1989.
[13] L. Gross, F. Mohn, N. Moll, P. Liljeroth, and G. Meyer, "The chemical structure of a molecule resolved by atomic force microscopy.," *Science (80-.).*, vol. 325, no. 5944, pp. 1110–1114, Aug. 2009.
[14] M. S. Rana, H. R. Pota, and I. R. Petersen, "Spiral Scanning With Improved Control for Faster Imaging of AFM," *IEEE Trans. Nanotechnol.*, vol. 13, no. 3, pp. 541–550, 2014.
[15] I. a. Mahmood and S. O. R. Moheimani, "Spiral scanning: An alternative to conventional raster scanning in high-speed scanning probe microscopes," *2010 Am. Control Conf.*, pp. 5757–5762, 2010.
[16] T. Tuma, J. Lygeros, V. Kartik, A. Sebastian, and A. Pantazi, "High-speed multiresolution scanning probe microscopy based on Lissajous scan trajectories.," *Nanotechnology*, vol. 23, no. 18, pp. 185501–9, May 2012.
[17] S. Z. Sullivan, R. D. Muir, J. A. Newman, M. S. Carlsen, S. Sreehari, C. Doerge, N. J. Begue, R. M. Everly, C. A. Bouman, and G. J. Simpson, "High frame-rate multichannel beam-scanning microscopy based on Lissajous trajectories," *Opt. Express*, vol. 22, no. 20, pp. 24224–34, Oct. 2014.
[18] A. Bazaei, Y. K. Yong, and S. O. R. Moheimani, "High-speed Lissajous-scan atomic force microscopy: scan pattern planning and control design issues.," *Rev. Sci. Instrum.*, vol. 83, no. 6, pp. 063701–10, Jun. 2012.
[19] G. Meyer and N. M. Amer, "Novel optical approach to atomic force

microscopy," *Appl. Phys. Lett.*, vol. 53, no. 12, pp. 1045–1047, 1988.
[20] P. K. Hansma, J. P. Cleveland, M. Radmacher, D. A. Walters, P. E. Hillner, M. Bezanilla, M. Fritz, D. Vie, H. G. Hansma, C. B. Prater, J. Massie, L. Fukunaga, J. Gurley, and V. Elings, "Tapping mode atomic force microscopy in liquids," *Appl. Phys. Lett.*, vol. 64, no. 13, pp. 1738–1740, Mar. 1994.
[21] Q. Zhong, D. Inniss, K. Kjoller, and V. B. Elings, "Fractured polymer/silica fiber surface studied by tapping mode atomic force microscopy," *Surf. Sci. Lett.*, vol. 290, no. 1–2, pp. L688–L692, Jun. 1993.
[22] F. J. Giessibl, "Atomic resolution on Si(111)-(7×7) by noncontact atomic force microscopy with a force sensor based on a quartz tuning fork," *Appl. Phys. Lett.*, vol. 76, no. 11, pp. 1470–1472, Mar. 2000.
[23] J. L. Bosse, S. Lee, A. S. Andersen, D. S. Sutherland, and B. D. Huey, "High speed friction microscopy and nanoscale friction coefficient mapping," *Meas. Sci. Technol.*, vol. 25, no. 11, pp. 115401–9, Nov. 2014.
[24] N. S. Tambe and B. Bhushan, "A new atomic force microscopy based technique for studying nanoscale friction at high sliding velocities," *J. Phys. D. Appl. Phys.*, vol. 38, no. 5, pp. 764–773, Mar. 2005.
[25] N. S. Tambe and B. Bhushan, "Scale dependence of micro/nano-friction and adhesion of MEMS/NEMS materials, coatings and lubricants," *Nanotechnology*, vol. 15, no. 11, pp. 1561–1570, Nov. 2004.
[26] Z. Wei, C. Wang, and C. Bai, "Investigation of Nanoscale Frictional Contact by Friction Force Microscopy," *Langmuir*, vol. 17, no. 13, pp. 3945–3951, 2001.
[27] M. F. Paige, "A comparison of atomic force microscope friction and phase imaging for the characterization of an immiscible polystyrene/poly(methyl methacrylate) blend film," *Polymer (Guildf).*, vol. 44, pp. 6345–6352, 2003.
[28] F. Moreno-Herrero, J. Colchero, J. Gómez-Herrero, and A. M. Baró, "Atomic force microscopy contact, tapping, and jumping modes for imaging biological samples in liquids," *Phys. Rev. E*, vol. 69, no. 3, pp. 031915–9, Mar. 2004.
[29] R. Proksch, "Multifrequency, repulsive-mode amplitude-modulated atomic force microscopy," *Appl. Phys. Lett.*, vol. 89, no. 11, pp. 1–4, 2006.
[30] L. Gross, F. Mohn, P. Liljeroth, J. Repp, F. J. Giessibl, and G. Meyer, "Measuring the charge state of an adatom with noncontact atomic force microscopy," *Science (80-.).*, vol. 324, no. 5933, pp. 1428–1431, 2009.
[31] G. Couturier, L. Nony, R. Boisgard, and J. P. Aimé, "Stability analysis of an oscillating tip-cantilever system in NC-AFM," *Appl. Surf. Sci.*, vol. 188, no. 3–4, pp. 341–348, 2002.
[32] J. Welker and F. J. Giessibl, "Revealing the Angular Symmetry of Chemical Bonds by Atomic Force Microscopy," *Science (80-.).*, vol. 336, no. 6080, pp. 444–449, Apr. 2012.
[33] M. Emmrich, F. Huber, F. Pielmeier, J. Welker, T. Hofmann, M. Schneiderbauer, D. Meuer, S. Polesya, S. Mankovsky, D. Kodderitzsch, H. Ebert, and F. J. Giessibl, "Subatomic resolution force microscopy reveals internal structure and adsorption sites of small iron clusters," *Science (80-.).*, vol. 348, no. 6232, pp.

308–311, Mar. 2015.
[34] T. R. Albrecht and S. Akamine, “Microfabrication of cantilever styli for the atomic force microscope,” *J. Vac. Sci. Technol. A*, vol. 8, no. 4, pp. 3386–3396, 1990.
[35] I. W. Rangelow, F. Shi, P. Hudek, T. Gotszalk, P. B. Grabiec, and P. Dumania, “Fabrication of piezoresistive-sensed AFM cantilever probe with integrated tip,” in *Proc. SPIE 2879, Micromachining and Microfabrication Process Technology II, 56*, 1996, pp. 56–64.
[36] D. J. Taatjes, a S. Quinn, M. R. Lewis, and E. G. Bovill, “Quality assessment of atomic force microscopy probes by scanning electron microscopy: correlation of tip structure with rendered images,” *Microsc. Res. Tech.*, vol. 44, no. 5, pp. 312–326, 1999.
[37] L. W. Francis, P. D. Lewis, C. J. Wright, and R. S. Conlan, “Atomic force microscopy comes of age,” *Biol. cell*, vol. 102, no. 2, pp. 133–143, 2010.
[38] S. Liu and Y. Wang, “A review of the application of atomic force microscopy (AFM) in food science and technology,” in *Advances in food and nutrition research*, vol. 62, 2011, pp. 201–40.
[39] J. M. Wallace, “Applications of atomic force microscopy for the assessment of nanoscale morphological and mechanical properties of bone,” *Bone*, vol. 50, no. 1, pp. 420–427, Jan. 2012.
[40] R. Garcia and E. T. Herruzo, “The emergence of multifrequency force microscopy,” *Nat. Nanotechnol.*, vol. 7, no. 4, pp. 217–226, Apr. 2012.
[41] M. Chyasnavichyus, S. L. Young, and V. V. Tsukruk, “Recent advances in micromechanical characterization of polymer, biomaterial, and cell surfaces with atomic force microscopy,” *Jpn. J. Appl. Phys.*, vol. 54, no. 8S2, pp. 08LA02–13, Aug. 2015.
[42] S. Hosaka, K. Etoh, A. Kikukawa, and H. Koyanagi, “Megahertz silicon atomic force microscopy (AFM) cantilever and high-speed readout in AFM-based recording,” *J. Vac. Sci. Technol. B Microelectron. Nanom. Struct.*, vol. 18, no. 1, pp. 94–99, 2000.
[43] G. T. Paloczi, B. L. Smith, P. K. Hansma, D. a. Walters, and M. a. Wendman, “Rapid imaging of calcite crystal growth using atomic force microscopy with small cantilevers,” *Appl. Phys. Lett.*, vol. 73, no. 12, pp. 1658–1660, 1998.
[44] T. Ando, “High-speed atomic force microscopy coming of age,” *Nanotechnology*, vol. 23, no. 6, pp. 062001–27, 2012.
[45] C. Braunsmann and T. E. Schäffer, “High-speed atomic force microscopy for large scan sizes using small cantilevers,” *Nanotechnology*, vol. 21, no. 22, pp. 225705–7, 2010.
[46] T. Fukuma and S. P. Jarvis, “Development of liquid-environment frequency modulation atomic force microscope with low noise deflection sensor for cantilevers of various dimensions,” *Rev. Sci. Instrum.*, vol. 77, no. 4, pp. 043701–8, 2006.
[47] A. Labuda, T. Brastaviceanu, I. Pavlov, W. Paul, and D. E. Rassier, “Optical

detection system for probing cantilever deflections parallel to a sample surface," *Rev. Sci. Instrum.*, vol. 82, no. 1, pp. 59–62, 2011.
[48] G. Meyer and N. M. Amer, "Optical-beam-deflection atomic force microscopy: The NaCl (001) surface," *Appl. Phys. Lett.*, vol. 56, no. 21, pp. 2100–2101, 1990.
[49] O. D. Payton, L. Picco, M. J. Miles, M. E. Homer, and A. R. Champneys, "Improving the signal-to-noise ratio of high-speed contact mode atomic force microscopy," *Rev. Sci. Instrum.*, vol. 83, no. 8, pp. 083710–4, Aug. 2012.
[50] H. I. Rasool, P. R. Wilkinson, A. Z. Stieg, and J. K. Gimzewski, "A low noise all-fiber interferometer for high resolution frequency modulated atomic force microscopy imaging in liquids," *Rev. Sci. Instrum.*, vol. 81, no. 2, pp. 023703–10, Feb. 2010.
[51] C. Leung, A. Bestembayeva, R. Thorogate, J. Stinson, A. Pyne, C. Marcovich, J. Yang, U. Drechsler, M. Despont, T. Jankowski, M. Tschöpe, and B. W. Hoogenboom, "Atomic force microscopy with nanoscale cantilevers resolves different structural conformations of the DNA double helix," *Nano Lett.*, vol. 12, no. 7, pp. 3846–50, 2012.
[52] P. C. Paul, A. W. Knoll, F. Holzner, M. Despont, and U. Duerig, "Rapid turnaround scanning probe nanolithography," *Nanotechnology*, vol. 22, no. 27, pp. 275306–9, Jul. 2011.
[53] O. D. Payton, L. Picco, D. Robert, A. Raman, M. E. Homer, A. R. Champneys, and M. J. Miles, "High-speed atomic force microscopy in slow motion—understanding cantilever behaviour at high scan velocities," *Nanotechnology*, vol. 23, no. 20, pp. 205704–6, 2012.
[54] O. D. Payton, L. Picco, A. R. Champneys, M. E. Homer, M. J. Miles, and A. Raman, "Experimental observation of contact mode cantilever dynamics with nanosecond resolution," *Rev. Sci. Instrum.*, vol. 82, no. 4, pp. 043704–5, 2011.
[55] M. Spletzer, A. Raman, and R. Reifenberger, "Spatio-temporal dynamics of microcantilevers tapping on samples observed under an atomic force microscope integrated with a scanning laser Doppler vibrometer: applications to proper orthogonal decomposition and model reduction," *J. Micromechanics Microengineering*, vol. 20, no. 8, pp. 085024–12, 2010.
[56] H.-S. Liao, K.-Y. Huang, I.-S. Hwang, T.-J. Chang, W. W. Hsiao, H.-H. Lin, E.-T. Hwu, and C.-S. Chang, "Operation of astigmatic-detection atomic force microscopy in liquid environments," *Rev. Sci. Instrum.*, vol. 84, no. 10, pp. 103709–7, Oct. 2013.
[57] H.-S. Liao, Y.-H. Chen, R.-F. Ding, H.-F. Huang, W.-M. Wang, E.-T. Hwu, K.-Y. Huang, C.-S. Chang, and I.-S. Hwang, "High-speed atomic force microscope based on an astigmatic detection system," *Rev. Sci. Instrum.*, vol. 85, no. 10, pp. 103710–7, Oct. 2014.
[58] E.-T. Hwu, H. Illers, L. Jusko, and H.-U. Danzebrink, "A hybrid scanning probe microscope (SPM) module based on a DVD optical head," *Meas. Sci. Technol.*, vol. 20, no. 8, pp. 084005–8, 2009.
[59] S. H. Lee, "High precision deflection measurement of microcantilever in an

optical pickup head based atomic force microscopy," *Rev. Sci. Instrum.*, vol. 83, no. 11, pp. 113703–4, Nov. 2012.
[60] K. W. Wee, G. Y. Kang, J. Park, J. Y. Kang, D. S. Yoon, J. H. Park, and T. S. Kim, "Novel electrical detection of label-free disease marker proteins using piezoresistive self-sensing micro-cantilevers," *Biosens. Bioelectron.*, vol. 20, pp. 1932–1938, Apr. 2005.
[61] G. E. Fantner, W. Schumann, R. J. Barbero, A. Deutschinger, V. Todorov, D. S. Gray, a M. Belcher, I. W. Rangelow, and K. Youcef-Toumi, "Use of self-actuating and self-sensing cantilevers for imaging biological samples in fluid," *Nanotechnology*, vol. 20, no. 43, pp. 434003–10, 2009.
[62] I. Soltani Bozchalooi and K. Youcef-Toumi, "Multi-actuation and PI control: a simple recipe for high-speed and large-range atomic force microscopy," *Ultramicroscopy*, vol. 146, pp. 117–124, Nov. 2014.
[63] G. Schitter, R. W. Stark, and A. Stemmer, "Fast contact-mode atomic force microscopy on biological specimen by model-based control," *Ultramicroscopy*, vol. 100, no. 3, pp. 253–257, Aug. 2004.
[64] G. Schitter, F. Allgöwer, and a Stemmer, "A new control strategy for high-speed atomic force miciroscopy," *Nanotechnology*, vol. 15, no. 1, pp. 108–114, Jan. 2004.
[65] O. Payton, A. R. Champneys, M. E. Homer, L. Picco, and M. J. Miles, "Feedback-induced instability in tapping mode atomic force microscopy: theory and experiment," *Proc. R. Soc. A Math. Phys. Eng. Sci.*, vol. 467, no. 2130, pp. 1801–1822, Dec. 2011.
[66] N. Kodera, M. Sakashita, and T. Ando, "Dynamic proportional-integral-differential controller for high-speed atomic force microscopy," *Rev. Sci. Instrum.*, vol. 77, pp. 083704–7, 2006.
[67] L. Picco, L. Bozec, A. Ulcinas, D. J. Engledew, M. Antognozzi, M. Horton, and M. J. Miles, "Breaking the speed limit with atomic force microscopy," *Nanotechnology*, vol. 18, no. 4, pp. 044030–4, Jan. 2007.
[68] "NanoWorld AG, Arrow NC Probes." 2016.
[69] Bruker, "Bruker, MSNL Probes," *Bruker MSNL Probes*, 2016. [Online]. Available: http://www.brukerafmprobes.com/p-3710-msnl-10.aspx.
[70] "NanoWorldAG, Arrow UHFAuD Probes," 2016. [Online]. Available: http://www.nanoworld.com/ultra-high-frequency-afm-tip-arrow-uhf-aud.
[71] J. D. Adams, A. Nievergelt, B. W. Erickson, C. Yang, M. Dukic, and G. E. Fantner, "High-speed imaging upgrade for a standard sample scanning atomic force microscope using small cantilevers," *Rev. Sci. Instrum.*, vol. 85, pp. 093702–7, 2014.
[72] K. Noi, D. Yamamoto, S. Nishikori, K. I. Arita-Morioka, T. Kato, T. Ando, and T. Ogura, "High-speed atomic force microscopic observation of ATP-dependent rotation of the AAA+ chaperone p97," *Structure*, vol. 21, no. 11, pp. 1992–2002, Nov. 2013.
[73] Y. Suzuki, N. Sakai, A. Yoshida, Y. Uekusa, A. Yagi, Y. Imaoka, S. Ito, K. Karaki,

and K. Takeyasu, “High-speed atomic force microscopy combined with inverted optical microscopy for studying cellular events,” *Sci. Rep.*, vol. 3, pp. 2131–7, Jan. 2013.

[74] Y. K. Yong, S. O. R. Moheimani, B. J. Kenton, and K. K. Leang, “Invited review article: high-speed flexure-guided nanopositioning: mechanical design and control issues,” *Rev. Sci. Instrum.*, vol. 83, no. 12, pp. 121101–22, Dec. 2012.

[75] S. P. Wadikhaye, Y. K. Yong, and S. O. R. Moheimani, “Design of a compact serial-kinematic scanner for high-speed atomic force microscopy: an analytical approach,” *Micro Nano Lett.*, vol. 7, no. 4, pp. 309–313, 2012.

[76] T. Tuma, “The Four Pillars of Nanopositioning for Scanning Probe Microscopy,” ETH Zurich, 2013.

[77] P. Klapetek, L. Picco, O. Payton, A. Yacoot, and M. Miles, “Error mapping of high-speed AFM systems,” *Meas. Sci. Technol.*, vol. 24, no. 2, pp. 25006–7, Feb. 2013.

[78] P. Klapetek, M. Valtr, L. Picco, O. D. Payton, J. Martinek, A. Yacoot, and M. J. Miles, “Large area high-speed metrology SPM system.,” *Nanotechnology*, vol. 26, no. 6, pp. 065501–9, Jan. 2015.

[79] Y. Chen, J. Cai, M. Liu, G. Zeng, Q. Feng, and Z. Chen, “Research on double-probe, double- and triple-tip effects during atomic force microscopy scanning,” *Scanning*, vol. 26, no. 4, pp. 155–161, 2004.

[80] J. P. Killgore, R. H. Geiss, and D. C. Hurley, “Continuous measurement of atomic force microscope tip wear by contact resonance force microscopy.,” *Small*, vol. 7, no. 8, pp. 1018–1022, Apr. 2011.

[81] R. C. Barrett and C. F. Quate, “High-speed, large-scale imaging with the atomic force microscope,” *J. Vac. Sci. Technol. B Microelectron. Nanom. Struct.*, vol. 9, no. 2, pp. 302–306, Mar. 1991.

[82] P. K. Hansma, G. Schitter, G. E. Fantner, and C. Prater, “Applied physics: High-speed atomic force microscopy,” *Science (80-.).*, vol. 314, no. 5799, pp. 601–602, Oct. 2006.

[83] T. Ando, “High-speed atomic force microscopy,” *Microscopy*, vol. 62, no. 1, pp. 81–93, Feb. 2013.

[84] S. Kuwajima, S. Horie, T. Horiuchi, H. Yamada, K. Matsushige, and K. Ishida, “Crystal and Layer Structures of Ferroelectric Oligomer Thin Films,” *Macromolecules*, vol. 42, no. 9, pp. 3353–3357, 2009.

[85] A. M. Adamska, R. Springell, A. D. Warren, L. Picco, O. Payton, and T. B. Scott, “Growth and characterization of uranium–zirconium alloy thin films for nuclear industry applications,” *J. Phys. D. Appl. Phys.*, vol. 47, no. 31, pp. 315301–10, Aug. 2014.

[86] A. McPherson, A. J. Malkin, and Y. G. Kuznetsov, “Atomic Force Microscopy in the Study of Macromolecular Crystal Growth,” *Annu. Rev. Biophys. Biomol. Struct.*, vol. 29, no. 1, pp. 361–410, Jun. 2000.

[87] Y. G. Kuznetsov, A. J. Malkin, and A. McPherson, “AFM studies of the nucleation and growth mechanisms of macromolecular crystals,” *J. Cryst.*

Growth, vol. 196, no. 2–4, pp. 489–502, Jan. 1999.
[88] Y. Cao, M. Li, M. Cheng, J. Song, and Z. Hu, "An in situ AFM investigation on the morphology of the (100) growth interface of ZTS crystal," *J. Cryst. Growth*, vol. 388, pp. 22–28, Feb. 2014.
[89] P. E. Hillner, S. Manne, A. J. Gratz, and P. K. Hansma, "AFM images of dissolution and growth on a calcite crystal," *Ultramicroscopy*, vol. 42–44, pp. 1387–1393, Jul. 1992.
[90] T. Ando, N. Kodera, Y. Naito, T. Kinoshita, K. Furuta, and Y. Y. Toyoshima, "A High-speed Atomic Force Microscope for Studying Biological Macromolecules in Action," *ChemPhysChem*, vol. 4, no. 11, pp. 1196–1202, 2003.
[91] T. Ando, N. Kodera, E. Takai, D. Maruyama, K. Saito, and A. Toda, "A high-speed atomic force microscope for studying biological macromolecules," *Proc. Natl. Acad. Sci.*, vol. 98, no. 22, pp. 12468–12472, 2001.
[92] M. J. Rost, L. Crama, P. Schakel, E. Van Tol, G. B. E. M. Van Velzen-Williams, C. F. Overgauw, H. Ter Horst, H. Dekker, B. Okhuijsen, M. Seynen, A. Vijftigschild, P. Han, A. J. Katan, K. Schoots, R. Schumm, W. Van Loo, T. H. Oosterkamp, and J. W. M. Frenken, "Scanning probe microscopes go video rate and beyond," *Rev. Sci. Instrum.*, vol. 76, no. 5, pp. 053710–9, 2005.
[93] M. Shibata, T. Uchihashi, T. Ando, and R. Yasuda, "Long-tip high-speed atomic force microscopy for nanometer-scale imaging in live cells," *Sci. Rep.*, vol. 5, pp. 8724–7, Jan. 2015.
[94] T. Ando, "Molecular machines directly observed by high-speed atomic force microscopy," *FEBS Lett.*, vol. 587, no. 8, pp. 997–1007, Apr. 2013.
[95] I. Casuso, N. Kodera, C. Le Grimellec, T. Ando, and S. Scheuring, "Contact-mode high-resolution high-speed atomic force microscopy movies of the purple membrane," *Biophys. J.*, vol. 97, no. 5, pp. 1354–1361, Sep. 2009.
[96] T. Ando, "Control techniques in high-speed atomic force microscopy," *Proc. Am. Control Conf.*, no. 4586984, pp. 3194–3200, 2008.
[97] N. Kodera, H. Yamashita, and T. Ando, "Active damping of the scanner for high-speed atomic force microscopy," *Rev. Sci. Instrum.*, vol. 76, pp. 053708–5, 2005.
[98] T. Ando, T. Uchihashi, N. Kodera, D. Yamamoto, M. Taniguchi, A. Miyagi, and H. Yamashita, "High-speed atomic force microscopy for observing dynamic biomolecular processes," *J. Mol. Recognit.*, vol. 20, no. September, pp. 448–458, 2007.
[99] S. Fukuda, T. Uchihashi, and T. Ando, "Method of mechanical holding of cantilever chip for tip-scan high-speed atomic force microscope," *Rev. Sci. Instrum.*, vol. 86, no. 6, pp. 063703–7, 2015.
[100] T. Ando, T. Uchihashi, N. Kodera, D. Yamamoto, A. Miyagi, M. Taniguchi, and H. Yamashita, "High-speed AFM and nano-visualization of biomolecular processes," *Pflugers Arch. Eur. J. Physiol.*, vol. 456, pp. 211–225, 2008.
[101] H. Watanabe, T. Uchihashi, T. Kobashi, M. Shibata, J. Nishiyama, R. Yasuda, and T. Ando, "Wide-area scanner for high-speed atomic force microscopy," *Rev. Sci.*

Instrum., vol. 84, no. 5, pp. 053702–10, May 2013.
[102] N. Kodera, D. Yamamoto, R. Ishikawa, and T. Ando, "Video imaging of walking myosin V by high-speed atomic force microscopy," *Nature*, vol. 468, no. 7320, pp. 72–76, 2010.
[103] T. Ando, "High-speed AFM imaging," *Curr. Opin. Struct. Biol.*, vol. 28, pp. 63–68, Oct. 2014.
[104] T. Ando, T. Uchihashi, and T. Fukuma, "High-speed atomic force microscopy for nano-visualization of dynamic biomolecular processes," *Prog. Surf. Sci.*, vol. 83, no. 7–9, pp. 337–437, Nov. 2008.
[105] A. D. Mehta, R. S. Rock, M. Rief, J. A. Spudich, M. S. Mooseker, and R. E. Cheney, "Myosin-V is a processive actin-based motor," *Nature*, vol. 400, no. 6744, pp. 590–593, Aug. 1999.
[106] E. Lecuona, A. Minin, H. E. Trejo, J. Chen, A. P. Comellas, H. Sun, D. Grillo, O. E. Nekrasova, L. C. Welch, I. Szleifer, V. I. Gelfand, and J. I. Sznajder, "Myosin-Va restrains the trafficking of Na+/K+-ATPase-containing vesicles in alveolar epithelial cells," *J. Cell Sci.*, vol. 122, no. 21, pp. 3915–3922, Nov. 2009.
[107] T. Itani and J. J. Santillan, "Characterization of Photoresist Dissolution," *Appl. Phys. Express*, vol. 3, no. 6, pp. 061601–3, Jun. 2010.
[108] T. Itani, "A Comprehensive Review of EUV Resist Materials and Processing at Selete," *J. Photopolym. Sci. Technol.*, vol. 24, no. 2, pp. 111–118, Jul. 2011.
[109] L. N. Plummer, T. M. L. Wigley, and D. L. Parkhurst, "The kinetics of calcite dissolution in CO2-water systems at 5 degrees to 60 degrees C and 0.0 to 1.0 atm CO2," *Am. J. Sci.*, vol. 278, no. 2, pp. 179–216, Feb. 1978.
[110] C. R. Becker, K. E. Strawhecker, Q. P. McAllister, and C. A. Lundgren, "In situ atomic force microscopy of lithiation and delithiation of silicon nanostructures for lithium ion batteries," *ACS Nano*, vol. 7, no. 10, pp. 9173–9182, Oct. 2013.
[111] A. Pyne, W. Marks, L. Picco, P. Dunton, A. Ulcinas, M. Barbour, S. Jones, J. Gimzewski, and M. J. Miles, "High-speed atomic force microscopy of dental enamel dissolution in citric acid," *Arch. Histol. Cytol.*, vol. 72, no. 4–5, pp. 209–215, 2009.
[112] L. M. Picco, T. Scott, J. Reed, and O. D. Payton, "Contact mode high-speed AFM – current capabilities," *Submitt. to IOP Nanotechnol.*, 2015.
[113] L. Picco, P. G. Dunton, A. Ulcinas, D. J. Engledew, O. Hoshi, T. Ushiki, and M. J. Miles, "High-speed AFM of human chromosomes in liquid," *Nanotechnology*, vol. 19, no. 38, pp. 384018–6, Sep. 2008.
[114] A. Mikheikin, A. Olsen, K. Leslie, B. Mishra, J. K. Gimzewski, and J. Reed, "Atomic force microscopic detection enabling multiplexed low-cycle-number quantitative polymerase chain reaction for biomarker assays," *Anal. Chem.*, vol. 86, no. 13, pp. 6180–3, Jul. 2014.
[115] L. M. Picco, O. D. Payton, A. D. Warren, A. I. Martinez-ubeda, R. Burrows, S. R. Street, and T. B. Scott, "Using High Speed Atomic force Microscopy to observe corrosion in real-time," in *55th Corrosion Science Symposium*, 2014.
[116] P. R. Seré, J. D. Culcasi, C. I. Elsner, and A. R. Di Sarli, "Relationship between

texture and corrosion resistance in hot-dip galvanized steel sheets," *Surf. Coatings Technol.*, vol. 122, no. 2–3, pp. 143–149, Dec. 1999.
[117] S. R. Street, N. Mi, A. J. M. C. Cook, H. B. Mohammed-Ali, L. Guo, T. Rayment, and A. J. Davenport, "Atmospheric pitting corrosion of 304L stainless steel: the role of highly concentrated chloride solutions," *Faraday Discuss.*, vol. 180, pp. 251–265, Jan. 2015.
[118] S. R. Street, W. Xu, M. Amri, L. Guo, S. J. M. Glanvill, P. D. Quinn, J. F. W. Mosselmans, J. Vila-Comamala, C. Rau, T. Rayment, and A. J. Davenport, "The Effect of Nitrate on Salt Layers in Pitting Corrosion of 304L Stainless Steel," *J. Electrochem. Soc.*, vol. 162, no. 9, pp. C457–C464, Jun. 2015.
[119] Q. Xu, K. Gao, Y. Wang, and X. Pang, "Characterization of corrosion products formed on different surfaces of steel exposed to simulated groundwater solution," *Appl. Surf. Sci.*, vol. 345, pp. 10–17, Aug. 2015.
[120] T. Brinkmann, C. Naderipour, J. Pohlmann, J. Wind, T. Wolff, E. Esche, D. Müller, G. Wozny, and B. Hoting, "Pilot scale investigations of the removal of carbon dioxide from hydrocarbon gas streams using poly (ethylene oxide)–poly (butylene terephthalate) PolyActive^{TM} thin film composite membranes," *J. Memb. Sci.*, vol. 489, pp. 237–247, Sep. 2015.
[121] N. Chen, B. Reeja-Jayan, J. Lau, P. Moni, A. Liu, B. Dunn, and K. K. Gleason, "Nanoscale, conformal polysiloxane thin film electrolytes for three-dimensional battery architectures," *Mater. Horizons*, vol. 2, no. 3, pp. 309–314, Apr. 2015.
[122] J. K. Hobbs, C. Vasilev, and A. D. L. Humphris, "VideoAFM — a new tool for high speed surface analysis," *Analyst*, vol. 131, pp. 251–256, 2006.
[123] J. K. Hobbs, C. Vasilev, and A. D. L. Humphris, "Real time observation of crystallization in polyethylene oxide with video rate atomic force microscopy," *Polymer (Guildf).*, vol. 46, no. 23, pp. 10226–10236, Nov. 2005.
[124] P. Welch and M. Muthukumar, "Molecular Mechanisms of Polymer Crystallization from Solution," *Phys. Rev. Lett.*, vol. 87, no. 21, pp. 218302–4, Nov. 2001.
[125] J. P. K. Doye and D. Frenkel, "Crystallization of a polymer on a surface," *J. Chem. Phys.*, vol. 109, no. 22, pp. 10033–10041, Dec. 1998.
[126] J.-U. Sommer and G. Reiter, "Polymer crystallization in quasi-two dimensions. II. Kinetic models and computer simulations," *J. Chem. Phys.*, vol. 112, no. 9, pp. 4384–4393, Mar. 2000.
[127] G. F. Hays, "Now is the Time," 2015.
[128] G.-L. Song, "The Grand Challenges in Electrochemical Corrosion Research," *Front. Mater.*, vol. 1, no. 2, pp. 1–3, Mar. 2014.
[129] B. Zhao, Y. Song, S. Wang, B. Dai, L. Zhang, Y. Dong, J. Lü, and J. Hu, "Mechanical mapping of nanobubbles by PeakForce atomic force microscopy," *Soft Matter*, vol. 9, no. 37, pp. 8837–8843, Aug. 2013.
[130] A. Laferrere, R. Burrows, R. Clark, C. Glover, G. Williams, O. Payton, and L. Picco, "In Situ Imaging of Corrosion Processes in Nuclear Fuel Cladding," in *Eurocorr 2015*, 2015.

[131] P. Erazmus-Vignal, V. Vignal, S. Saedlou, and F. Krajcarz, “Corrosion behaviour of sites containing (Cr, Fe)2N particles in thermally aged duplex stainless steel studied using capillary techniques, atomic force microscopy and potentiostatic pulse testing method,” *Corros. Sci.*, vol. 99, pp. 194–204, Oct. 2015.
[132] L. Guan, B. Zhang, X. P. Yong, J. Q. Wang, E.-H. Han, and W. Ke, “Effects of cyclic stress on the metastable pitting characteristic for 304 stainless steel under potentiostatic polarization,” *Corros. Sci.*, vol. 93, pp. 80–89, Apr. 2015.
[133] N. Birbilis, K. Meyer, B. C. Muddle, and S. P. Lynch, “In situ measurement of corrosion on the nanoscale,” *Corros. Sci.*, vol. 51, no. 8, pp. 1569–1572, Aug. 2009.
[134] D. M. Carberry, L. Picco, P. G. Dunton, and M. J. Miles, “Mapping real-time images of high-speed AFM using multitouch control,” *Nanotechnology*, vol. 20, no. 43, pp. 434018–5, 2009.
[135] X. Li, W. Cai, J. An, S. Kim, J. Nah, D. Yang, R. Piner, A. Velamakanni, I. Jung, E. Tutuc, S. K. Banerjee, L. Colombo, and R. S. Ruoff, “Large-area synthesis of high-quality and uniform graphene films on copper foils,” *Science (80-.).*, vol. 324, no. 5932, pp. 1312–1314, Jun. 2009.
[136] M. Malloy, B. Thiel, B. D. Bunday, S. Wurm, M. Mukhtar, K. Quoi, T. Kemen, D. Zeidler, A. L. Eberle, T. Garbowski, G. Dellemann, and J. H. Peters, “Massively parallel E-beam inspection: enabling next-generation patterned defect inspection for wafer and mask manufacturing,” in *Proc. SPIE 9423, Alternative Lithographic Technologies VII*, 2015, p. 942319.
[137] J. C. Baena and Z. Peng, “3D quantitative characterization of degraded surfaces of human knee cartilages affected by osteoarthritis,” *Wear*, vol. 319, no. 1–2, pp. 1–11, Nov. 2014.
[138] A. Raman, “Recent advances in atomic force microscopy for nanobiological and nanocomposite applications,” 2010.
[139] C. H. Lui, L. Liu, K. F. Mak, G. W. Flynn, and T. F. Heinz, “Ultraflat graphene,” *Nature*, vol. 462, no. 7271, pp. 339–341, 2009.
[140] Y. Kubota, “New developments in electron microscopy for serial image acquisition of neuronal profiles,” *Microscopy*, vol. 64, no. 1, pp. 27–36, Feb. 2015.
[141] A. L. Eberle, S. Mikula, R. Schalek, J. Lichtman, M. L. K. Tate, and D. Zeidler, “High-resolution, high-throughput imaging with a multibeam scanning electron microscope,” *J. Microsc.*, vol. 259, no. 2, pp. 114–120, 2015.
[142] A. Dance, “Connectomes make the map,” *Nature*, vol. 526, no. 7571, pp. 147–149, Sep. 2015.
[143] P. Vettiger, G. Cross, M. Despont, U. Drechsler, U. Durig, B. Gotsmann, W. Haberle, M. a. Lantz, H. E. Rothuizen, R. Stutz, and G. K. Binnig, “The ‘millipede’ - nanotechnology entering data storage,” *IEEE Trans. Nanotechnol.*, vol. 1, no. 1, pp. 39–55, 2002.
[144] E. Eleftheriou, T. Antonakopoulos, G. K. Binnig, G. Cherubini, M. Despont, a. Dholakia, U. Durig, M. a. Lantz, H. Pozidis, H. E. Rothuizen, and P. Vettiger,

"Millipede - a MEMS-based scanning-probe data-storage system," *IEEE Trans. Magn.*, vol. 39, no. 2, pp. 938–945, 2003.
[145] M. Seong, S. Somnath, H. J. Kim, and W. P. King, "Parallel nanoimaging using an array of 30 heated microcantilevers," *RSC Adv.*, vol. 4, no. 47, pp. 24747–24754, Jun. 2014.
[146] R. Garcia, A. W. Knoll, and E. Riedo, "Advanced scanning probe lithography," *Nat. Nanotechnol.*, vol. 9, no. 8, pp. 577–587, Aug. 2014.
[147] S. C. Minne, G. Yaralioglu, S. R. Manalis, J. D. Adams, J. Zesch, a. Atalar, and C. F. Quate, "Automated parallel high-speed atomic force microscopy," *Appl. Phys. Lett.*, vol. 72, no. 18, pp. 2340–2342, 1998.
[148] S. Somnath, H. J. Kim, H. Hu, and W. P. King, "Parallel nanoimaging and nanolithography using a heated microcantilever array," *Nanotechnology*, vol. 25, no. 1, pp. 014001–12, Jan. 2014.
[149] T. V. Vorburger, J. A. Dagata, G. Wilkening, K. Lizuka, E. G. Thwaite, and P. Lonardo, "Industrial Uses of STM and AFM," *Ann. CIRP*, vol. 46, no. 2, pp. 597–620, 1997.
[150] G. Borionetti, A. Bazzali, and R. Orizio, "Atomic force microscopy: a powerful tool for surface defect and morphology inspection in semiconductor industry," *Eur. Phys. J. Appl. Phys.*, vol. 27, no. 1–3, pp. 101–106, Jul. 2004.
[151] U. Hubner, W. Morgenroth, H. G. Meyer, T. Sulzbach, B. Brendel, and W. Mirande, "Downwards to metrology in nanoscale: determination of the AFM tip shape with well-known sharp-edged calibration structures," *Appl. Phys. A Mater. Sci. Process.*, vol. 76, no. 6, pp. 913–917, Apr. 2003.
[152] P. Klapetek, M. Valtr, and M. Matula, "A long-range scanning probe microscope for automotive reflector optical quality inspection," *Meas. Sci. Technol.*, vol. 22, no. 9, pp. 094011–7, Sep. 2011.
[153] H. Barnard, C. Randall, D. Bridges, and P. K. Hansma, "The long range voice coil atomic force microscope," *Rev. Sci. Instrum.*, vol. 83, no. 2, pp. 023705–4, Feb. 2012.
[154] T. Mariani and C. Ascoli, "Comment on 'The long range voice coil atomic force microscope' [Rev. Sci. Instrum. 83, 023705 (2012)].," *Review of Scientific Instruments*, vol. 83, no. 9. AIP Publishing, p. 097103; author reply 097104, 18-Sep-2012.
[155] R. García Cantú and M. A. Huerta Garnica, "Inductoscanner tunneling microscope," *Surf. Sci.*, vol. 181, no. 1–2, pp. 216–221, Mar. 1987.
[156] T. Mariani, C. Frediani, and C. Ascoli, "A three-dimensional scanner for probe microscopy on the millimetre scale," *Appl. Phys. A Mater. Sci. Process.*, vol. 66, no. 7, pp. S861–S866, Mar. 1998.
[157] P. Klapetek, M. Valtr, V. Duchoň, and J. Sobota, "Voice coil-based scanning probe microscopy," *Nanoscale Res. Lett.*, vol. 7, no. 1, pp. 332–7, Jan. 2012.
[158] G. Dai, F. Zhu, and J. Fluegge, "High-speed metrological large range AFM," *Meas. Sci. Technol.*, vol. 26, no. 9, pp. 095402–10, 2015.
[159] G. Dai, F. Pohlenz, H.-U. Danzebrink, M. Xu, K. Hasche, and G. Wilkening,

"Metrological large range scanning probe microscope," *Rev. Sci. Instrum.*, vol. 75, no. 4, pp. 962–969, Mar. 2004.
[160] R. D. Boyd and A. Cuenat, "New analysis procedure for fast and reliable size measurement of nanoparticles from atomic force microscopy images," *J. Nanoparticle Res.*, vol. 13, no. 1, pp. 105–113, Jul. 2011.
[161] P. Klapetek, M. Valtr, D. Nečas, O. Salyk, and P. Dzik, "Atomic force microscopy analysis of nanoparticles in non-ideal conditions," *Nanoscale Res. Lett.*, vol. 6, no. 1, pp. 514–9, Jan. 2011.
[162] C. Ke, Y. Jiang, P. A. Mieczkowski, G. G. Muramoto, J. P. Chute, and P. E. Marszalek, "Nanoscale detection of ionizing radiation damage to DNA by atomic force microscopy," *Small*, vol. 4, no. 2, pp. 288–294, Feb. 2008.
[163] V. Charbois, J. Lebreton, M. Savoye, E. Labonne, A. Labourier, B. Dumont, C. Lenox, and M. von Den Hoff, "Defect reduction for 20nm high-k metal gate technology," in *ASMC 2015 26th Annual SEMI Advanced Semiconductor Manufacturing Conference*, 2015, pp. 14–18.
[164] S. Zhao and Q. Yang, "A Stitching Method for AFM Based Large Scale Scanning with High Resolution," in *World Congress*, 2014, vol. 19, no. 1, pp. 2697–2702.
[165] F. Marinello, P. Bariani, L. De Chiffre, and H. N. Hansen, "Development and analysis of a software tool for stitching three-dimensional surface topography data sets," *Meas. Sci. Technol.*, vol. 18, no. 5, pp. 1404–1412, May 2007.
[166] V. Rankov, R. J. Locke, R. J. Edens, and B. Vojnovic, "An algorithm for image stitching and blending," in *Proc. SPIE 5701, Three-Dimensional and Multidimensional Microscopy: Image Acquisition and Processing XII*, 2005, vol. 5701, no. March, pp. 190–199.
[167] S. C. Minne, J. D. Adams, G. Yaralioglu, S. R. Manalis, A. Atalar, and C. F. Quate, "Centimeter scale atomic force microscope imaging and lithography," *Appl. Phys. Lett.*, vol. 73, no. 12, pp. 1742–1744, 1998.
[168] O. D. Payton, "High-speed atomic force microscopy under the microscope," University of Bristol, 2012.
[169] P. Cullen, K. Cox, M. Bin Subhan, L. M. Picco, O. D. Payton, D. Buckley, S. Hodge, N. Skipper, V. Tileli, and C. Howard, "Ionic Solutions of 2-dimensional Materials," *Submitt. to Sci.*, 2016.
[170] P. Nemes-Incze, Z. Osváth, K. Kamarás, and L. P. Biró, "Anomalies in thickness measurements of graphene and few layer graphite crystals by tapping mode atomic force microscopy," *Carbon N. Y.*, vol. 46, no. 11, pp. 1435–1442, Sep. 2008.
[171] X. Jia, J. Campos-Delgado, M. Terrones, V. Meunier, and M. S. Dresselhaus, "Graphene edges: a review of their fabrication and characterization," *Nanoscale*, vol. 3, no. 1, pp. 86–95, Jan. 2011.
[172] M. P. Boneschanscher, J. van der Lit, Z. Sun, I. Swart, P. Liljeroth, and D. Vanmaekelbergh, "Quantitative atomic resolution force imaging on epitaxial graphene with reactive and nonreactive AFM probes," *ACS Nano*, vol. 6, no. 11, pp. 10216–10221, Nov. 2012.

[173] V. Korpelainen, J. Seppä, and A. Lassila, “Design and characterization of MIKES metrological atomic force microscope,” *Precis. Eng.*, vol. 34, no. 4, pp. 735–744, Oct. 2010.
[174] N. S. Tambe, “Nanotribological Investigations of Materials, Coatings and Lubricants for Nanotechnology Applications at High Sliding Velocities,” 2005.
[175] J. J. Roa, G. Oncins, J. Díaz, X. G. Capdevila, F. Sanz, and M. Segarra, “Study of the friction, adhesion and mechanical properties of single crystals, ceramics and ceramic coatings by AFM,” *J. Eur. Ceram. Soc.*, vol. 31, no. 4, pp. 429–449, 2011.
[176] K. van der Werf, C. Putman, B. de Grooth, and J. Greve, “Adhesion Force Imaging in Air and Liquid by Adhesion Mode Atomic Force Microscopy,” *Appl. Phys. Lett.*, vol. 65, no. 9, pp. 1195–1197, 1994.
[177] C. C. Dupont-Gillain and I. Jacquemart, “Patterned collagen layers on polystyrene: Direct probing using AFM in the adhesion mapping mode,” *Surf. Sci.*, vol. 539, no. 1–3, pp. 145–154, Aug. 2003.
[178] D. G. Yablon, A. Gannepalli, R. Proksch, J. Killgore, D. C. Hurley, J. Grabowski, and A. H. Tsou, “Quantitative viscoelastic mapping of polyolefin blends with contact resonance atomic force microscopy,” *Macromolecules*, vol. 45, no. 10, pp. 4363–4370, 2012.
[179] A. Kumar, U. Rabe, and W. Arnold, “Mapping of Elastic Stiffness in an α+β Titanium Alloy using Atomic Force Acoustic Microscopy,” *Jpn. J. Appl. Phys.*, vol. 47, no. 7, pp. 6077–6080, Jul. 2008.
[180] G. Stan, S. W. King, and R. F. Cook, “Nanoscale mapping of contact stiffness and damping by contact resonance atomic force microscopy,” *Nanotechnology*, vol. 23, no. 21, pp. 215703–9, Jun. 2012.
[181] J. a Turner and J. S. Wiehn, “Sensitivity of flexural and torsional vibration modes of atomic force microscope cantilevers to surface stiffness variations,” *Nanotechnology*, vol. 12, no. 3, pp. 322–330, 2001.
[182] A. Gannepalli, D. G. Yablon, A. H. Tsou, and R. Proksch, “Corrigendum: Mapping nanoscale elasticity and dissipation using dual frequency contact resonance AFM,” *Nanotechnology*, vol. 22, no. 35, p. 355705, 2011.
[183] X. Xu, J. Melcher, and A. Raman, “Accurate force spectroscopy in tapping mode atomic force microscopy in liquids,” *Phys. Rev. B*, vol. 81, no. 3, pp. 035407–7, 2010.
[184] X. Xu, J. Melcher, S. Basak, R. Reifenberger, and A. Raman, “Compositional contrast of biological materials in liquids using the momentary excitation of higher eigenmodes in dynamic atomic force microscopy,” *Phys. Rev. Lett.*, vol. 102, no. 6, pp. 060801–4, Feb. 2009.
[185] M. Kocun, A. Labuda, A. Gannepalli, and R. Proksch, “Contact resonance atomic force microscopy imaging in air and water using photothermal excitation,” *Rev. Sci. Instrum.*, vol. 86, no. 8, pp. 083706–5, Aug. 2015.
[186] A. Avila and B. Bhushan, “Electrical Measurement Techniques in Atomic Force Microscopy,” *Crit. Rev. Solid State Mater. Sci.*, vol. 35, no. 1, pp. 38–51, 2010.

[187] R. a Oliver, “Advances in AFM for the electrical characterization of semiconductors,” *Reports Prog. Phys.*, vol. 71, no. 7, pp. 076501–37, 2008.
[188] K. Edinger, T. Gotszalk, and I. W. Rangelow, “Novel high resolution scanning thermal probe,” *J. Vac. Sci. Technol. B Microelectron. Nanom. Struct.*, vol. 19, no. 6, pp. 2856–2860, 2001.
[189] O. D. Payton, L. Picco, T. Scott, A. Raman, J. E. Sader, J. Killgore, and D. C. Hurley, “Development of a high-speed contact resonance force microscope,” *Submitt. to IOP Nanotechnol.*, 2016.
[190] A. Warren, A. Martinez-Ubeda, O. Payton, L. Picco, and T. Scott, “Preparation of stainless steel surfaces for scanning probe microscopy,” *Micros. Today*, vol. 24, 2016.
[191] P. M. Ajayan, L. S. Schadler, and P. V. Braun, *Nanocomposite Science and Technology*. John Wiley & Sons, 2006.
[192] P. J. F. Harris, “Carbon nanotube composites,” *Int. Mater. Rev.*, vol. 49, no. 1, pp. 31–43, Jul. 2004.
[193] D. Qian, E. C. Dickey, R. Andrews, and T. Rantell, “Load transfer and deformation mechanisms in carbon nanotube-polystyrene composites,” *Appl. Phys. Lett.*, vol. 76, no. 20, pp. 2868–2870, May 2000.
[194] R. K. Gupta and N. Birbilis, “The influence of nanocrystalline structure and processing route on corrosion of stainless steel: A review,” *Corros. Sci.*, vol. 92, pp. 1–15, Mar. 2015.
[195] Y. Funakawa, T. Shiozaki, K. Tomita, T. Yamamoto, and E. Maeda, “Development of High Strength Hot-rolled Sheet Steel Consisting of Ferrite and Nanometer-sized Carbides,” *ISIJ Int.*, vol. 44, no. 11, pp. 1945–1951, May 2004.
[196] J. W. Park, H. C. Lee, and S. Lee, “Composition, microstructure, hardness, and wear properties of high-speed steel rolls,” *Metall. Mater. Trans. A*, vol. 30, no. 2, pp. 399–409, Feb. 1999.
[197] E. Badisch and C. Mitterer, “Abrasive wear of high speed steels: Influence of abrasive particles and primary carbides on wear resistance,” *Tribol. Int.*, vol. 36, no. 10, pp. 765–770, Oct. 2003.
[198] N. J. Petch, “The influence of grain boundary carbide and grain size on the cleavage strength and impact transition temperature of steel,” *Acta Metall.*, vol. 34, no. 7, pp. 1387–1393, Jul. 1986.
[199] A. E. Ennos, “The origin of specimen contamination in the electron microscope,” *Br. J. Appl. Phys.*, vol. 4, no. 4, pp. 101–106, Apr. 1953.
[200] S. K. Ray and O. N. Mohanty, “TEM Investigation of Carbide Precipitation in Low Carbon Steels Containing Silicon,” *Trans. Japan Inst. Met.*, vol. 24, no. 2, pp. 81–87, Jun. 1983.
[201] J. T. Tchuindjang and J. Lecomte-Beckers, “Use of microscopy for identification of complex MC, M2C, M7C3, M6C and M23C6 carbides in high-speed steels,” Jan. 2005.
[202] M. Hayakawa, S. Matsuoka, and K. Tsuzaki, “Microstructural Analyses of Grain Boundary Carbides of Tempered Martensite in Medium-Carbon Steel by

Atomic Force Microscopy," *Mater. Trans.*, vol. 43, no. 7, pp. 1758–1766, Sep. 2002.
[203] S. R. Cohen and E. Kalfon-Cohen, "Dynamic nanoindentation by instrumented nanoindentation and force microscopy: a comparative review.," *Beilstein J. Nanotechnol.*, vol. 4, pp. 815–33, Jan. 2013.
[204] O. D. Payton, L. Picco, A. Martinez-Ubeda, A. Warren, and T. B. Scott, "The continuing development of High-Speed Atomic Force Microscopy for use with EDF steel samples," Bristol, 2014.
[205] V. Matsagar, Ed., *Advances in Structural Engineering*. New Delhi: Springer India, 2015.
[206] C. Haase, M. Kühbach, L. A. Barrales-Mora, S. L. Wong, F. Roters, D. A. Molodov, and G. Gottstein, "Recrystallization behavior of a high-manganese steel: Experiments and simulations," *Acta Mater.*, vol. 100, pp. 155–168, Nov. 2015.
[207] D. S. Svyetlichnyy, K. Muszka, and J. Majta, "Three-dimensional frontal cellular automata modeling of the grain refinement during severe plastic deformation of microalloyed steel," *Comput. Mater. Sci.*, vol. 102, pp. 159–166, May 2015.
[208] S. Hutterer, S. Mayr, G. Zauner, R. Silye, and K. Schilcher, "Data mining supported analysis of medical atomic force microscopy images," in *2013 IEEE Symposium on Computational Intelligence in Healthcare and e-health (CICARE)*, 2013, pp. 99–104.
[209] J. P. Killgore, D. G. Yablon, A. H. Tsou, A. Gannepalli, P. a. Yuya, J. a. Turner, R. Proksch, and D. C. Hurley, "Viscoelastic property mapping with contact resonance force microscopy," *Langmuir*, vol. 27, no. 23, pp. 13983–13987, 2011.
[210] J. P. Killgore and D. C. Hurley, "Low-force AFM nanomechanics with higher-eigenmode contact resonance spectroscopy," *Nanotechnology*, vol. 23, no. 5, pp. 055702–10, Feb. 2012.
[211] G. Stan and R. F. Cook, "Mapping the elastic properties of granular Au films by contact resonance atomic force microscopy," *Nanotechnology*, vol. 19, no. 23, pp. 235701–10, Jun. 2008.
[212] P. A. Yuya, D. C. Hurley, and J. A. Turner, "Contact-resonance atomic force microscopy for viscoelasticity," *J. Appl. Phys.*, vol. 104, no. 7, pp. 074916–7, 2008.
[213] J. R. Lozano, D. Kiracofe, J. Melcher, R. Garcia, and A. Raman, "Calibration of higher eigenmode spring constants of atomic force microscope cantilevers," *Nanotechnology*, vol. 21, pp. 465502–7, 2010.
[214] MatWeb, "MatWeb." [Online]. Available: http://www.matweb.com. [Accessed: 21-Sep-2015].
[215] M. Göken and M. Kempf, "Microstructural properties of superalloys investigated by nanoindentations in an atomic force microscope," *Acta Mater.*, vol. 47, no. 3, pp. 1043–1052, 1999.
[216] W. C. Oliver and G. M. Pharr, "Nanoindentation in materials research: Past ,

present , and future," *MRS Bull.*, vol. 35, no. November, pp. 897–907, 2010.
[217] X. Li, Z. Li, X. F. Tao, L. L. Ren, S. T. Gao, and G. F. Xu, "Distribution of residual strain around nanoindentations in silicon," *Mater. Lett.*, vol. 132, no. September, pp. 285–289, Oct. 2014.
[218] D. Allen, "Analysis of silicon wafer damage due to nanoindentation by microraman spectroscopy and white beam synchrotron X-ray toporaphy," Dublin City University. School of Electronic Engineering, 2014.
[219] C. Braunsmann, J. Seifert, J. Rheinlaender, and T. E. Schäffer, "High-speed force mapping on living cells with a small cantilever atomic force microscope," *Rev. Sci. Instrum.*, vol. 85, no. 7, pp. 073703–8, Jul. 2014.
[220] O. Kolosov, A. Gruverman, J. Hatano, K. Takahashi, and H. Tokumoto, "Nanoscale visualization and control of ferroelectric domains by atomic force microscopy," *Phys. Rev. Lett.*, vol. 74, no. 21, pp. 4309–4312, May 1995.
[221] H. J. Butt, B. Cappella, and M. Kappl, "Force measurements with the atomic force microscope: Technique, interpretation and applications," *Surf. Sci. Rep.*, vol. 59, no. 1–6, pp. 1–152, 2005.
[222] A. Gruverman, O. Auciello, and H. Tokumoto, "Scanning force microscopy for the study of domain structure in ferroelectric thin films," *J. Vac. Sci. Technol. B Microelectron. Nanom. Struct.*, vol. 14, no. 2, pp. 602–605, Mar. 1996.
[223] R. Nath, Y. H. Chu, N. a. Polomoff, R. Ramesh, and B. D. Huey, "High speed piezoresponse force microscopy: less than 1 frame per second nanoscale imaging," *Appl. Phys. Lett.*, vol. 93, no. 7, pp. 072905–3, 2008.
[224] R. Álvarez-Asencio, J. Pan, E. Thormann, and M. W. Rutland, "Tribological Properties Mapping: Local Variation in Friction Coefficient and Adhesion," *Tribol. Lett.*, vol. 50, no. 3, pp. 387–395, Apr. 2013.
[225] J. E. Sader, J. A. Sanelli, B. D. Adamson, J. P. Monty, X. Wei, S. A. Crawford, J. R. Friend, I. Marusic, P. Mulvaney, and E. J. Bieske, "Spring constant calibration of atomic force microscope cantilevers of arbitrary shape," *Rev. Sci. Instrum.*, vol. 83, no. 10, pp. 103705–16, Oct. 2012.
[226] J. E. Sader, I. Larson, P. Mulvaney, and L. R. White, "Method for the calibration of atomic force microscope cantilevers," *Rev. Sci. Instrum.*, vol. 66, no. July, pp. 3789–3798, 1995.
[227] O. D. Payton, L. Picco, M. J. Miles, M. E. Homer, and A. R. Champneys, "Modelling oscillatory flexure modes of an atomic force microscope cantilever in contact mode whilst imaging at high speed," *Nanotechnology*, vol. 23, no. 26, pp. 265702–7, Jul. 2012.
[228] D. Kiracofe and A. Raman, "On eigenmodes, stiffness, and sensitivity of atomic force microscope cantilevers in air versus liquids," *J. Appl. Phys.*, vol. 107, no. 3, pp. 033506–9, 2010.
[229] E. S. Snow, P. M. Campbell, and F. K. Perkins, "High speed patterning of a metal silicide using scanned probe lithography," *Appl. Phys. Lett.*, vol. 75, no. 10, pp. 1476–1478, 1999.
[230] A. a. Tseng, A. Notargiacomo, and T. P. Chen, "Nanofabrication by scanning

probe microscope lithography: A review," *J. Vac. Sci. Technol. B Microelectron. Nanom. Struct.*, vol. 23, no. 3, pp. 877–894, 2005.
[231] R. Garcia, R. V Martinez, and J. Martinez, "Nano-chemistry and scanning probe nanolithographies," *Chem. Soc. Rev.*, vol. 35, no. 1, pp. 29–38, Jan. 2006.
[232] L. G. Rosa and J. Liang, "Atomic force microscope nanolithography: dip-pen, nanoshaving, nanografting, tapping mode, electrochemical and thermal nanolithography," *J. Phys. Condens. Matter*, vol. 21, no. 48, pp. 483001–18, Dec. 2009.
[233] R. D. Piner, J. Zhu, F. Xu, S. H. Hong, and C. A. Mirkin, "'Dip-pen' nanolithography," *Science (80-.).*, vol. 283, no. 5402, pp. 661–663, 1999.
[234] C. Obermair, A. Wagner, and T. Schimmel, "The atomic force microscope as a mechano–electrochemical pen," *Beilstein J. Nanotechnol.*, vol. 2, pp. 659–664, Jan. 2011.
[235] P. Mesquida, E. M. Blanco, and R. A. McKendry, "Patterning amyloid peptide fibrils by AFM charge writing," *Langmuir*, vol. 22, no. 22, pp. 9089–9091, 2006.
[236] N. S. Losilla, J. Martinez, E. Bystrenova, P. Greco, F. Biscarini, and R. García, "Patterning pentacene surfaces by local oxidation nanolithography," *Ultramicroscopy*, vol. 110, no. 6, pp. 729–732, May 2010.
[237] R. Garcıia, M. Calleja, and H. Rohrer, "Patterning of silicon surfaces with noncontact atomic force microscopy: Field-induced formation of nanometer-size water bridges," *J. Appl. Phys.*, vol. 86, no. 4, pp. 1898–1903, 1999.
[238] D. Stievenard, P. Fontaine, and E. Dubois, "Nanooxidation using a scanning probe microscope: An analytical model based on field induced oxidation," *Appl. Phys. Lett.*, vol. 70, no. 24, pp. 3272–3274, 1997.
[239] M. Tello and R. García, "Nano-oxidation of silicon surfaces: Comparison of noncontact and contact atomic-force microscopy methods," *Appl. Phys. Lett.*, vol. 79, no. 3, pp. 424–426, 2001.
[240] H. C. Day and D. R. Allee, "Selective area oxidation of silicon with a scanning force microscope," *Appl. Phys. Lett.*, vol. 62, no. 21, pp. 2691–2693, May 1993.
[241] J. A. Vicary and M. J. Miles, "Pushing the boundaries of local oxidation nanolithography: Short timescales and high speeds," *Ultramicroscopy*, vol. 108, no. 10, pp. 1120–1123, Sep. 2008.
[242] Y.-S. Choi, X. Wu, and D.-W. Lee, "Selective nano-patterning of graphene using a heated atomic force microscope tip," *Rev. Sci. Instrum.*, vol. 85, no. 4, pp. 045002–9, Apr. 2014.
[243] W.-K. Lee, M. Haydell, J. T. Robinson, A. R. Laracuente, E. Cimpoiasu, W. P. King, and P. E. Sheehan, "Nanoscale reduction of graphene fluoride via thermochemical nanolithography," *ACS Nano*, vol. 7, no. 7, pp. 6219–6224, Jul. 2013.
[244] R. Szoszkiewicz, T. Okada, S. C. Jones, T.-D. Li, W. P. King, S. R. Marder, and E. Riedo, "High-speed, sub-15 nm feature size thermochemical nanolithography," *Nano Lett.*, vol. 7, no. 4, pp. 1064–1069, Apr. 2007.
[245] J. A. Dagata, C. Martin, H. Kuramochi, H. Yokoyama, and I. Introduction,

"Current, charge, and capacitance during scanning probe oxidation of silicon. I. Maximum charge density and lateral diffusion," *J. Appl. Phys.*, vol. 96, no. 4, pp. 2386–2392, 2004.

[246] F. Pérez-Murano, K. Birkelund, K. Morimoto, and J. A. Dagata, "Voltage modulation scanned probe oxidation," *Appl. Phys. Lett.*, vol. 75, no. 2, pp. 199–201, 1999.

[247] J. A. Dagata, J. Schneir, H. H. Harary, C. J. Evans, M. T. Postek, and J. Bennett, "Modification of hydrogen-passivated silicon by a scanning tunneling microscope operating in air," *Appl. Phys. Lett.*, vol. 56, no. 20, pp. 2001–2003, 1990.

[248] R. V Martínez, J. Martínez, and R. Garcia, "Silicon nanowire circuits fabricated by AFM oxidation nanolithography," *Nanotechnology*, vol. 21, no. 24, pp. 245301–5, Jun. 2010.

[249] Z. Wei, D. Wang, S. Kim, S.-Y. Kim, Y. Hu, M. K. Yakes, A. R. Laracuente, Z. Dai, S. R. Marder, C. Berger, W. P. King, W. A. de Heer, P. E. Sheehan, and E. Riedo, "Nanoscale tunable reduction of graphene oxide for graphene electronics," *Science (80-.).*, vol. 328, no. 5984, pp. 1373–1376, Jun. 2010.

[250] X. N. Xie, H. J. Chung, C. H. Sow, and A. T. S. Wee, "Nanoscale materials patterning and engineering by atomic force microscopy nanolithography," *Mater. Sci. Eng. R Reports*, vol. 54, no. 1–2, pp. 1–48, 2006.

[251] K. Lee, S. Park, C. A. Mirkin, J. C. Smith, and M. Mrksich, "Protein Nanoarrays Generated By Dip-Pen Nanolithography," *Science (80-.).*, vol. 295, pp. 1702–1705, 2002.

[252] R. van Oorschot, H. Perez Garza, R. J. S. Derks, U. Staufer, and M. Ghatkesar, "A microfluidic AFM cantilever based dispensing and aspiration platform," *EPJ Tech. Instrum.*, vol. 2, no. 1, pp. 1–11, Mar. 2015.

[253] K. Salaita, Y. Wang, J. Fragala, R. A. Vega, C. Liu, and C. A. Mirkin, "Massively parallel dip-pen nanolithography with 55000-pen two-dimensional arrays," *Angew. Chemie (International ed.)*, vol. 45, no. 43, pp. 7220–7223, Nov. 2006.

[254] F. Brinkmann, M. Hirtz, A. M. Greiner, M. Weschenfelder, B. Waterkotte, M. Bastmeyer, and H. Fuchs, "Interdigitated multicolored bioink micropatterns by multiplexed polymer pen lithography," *Small*, vol. 9, no. 19, pp. 3266–3275, Oct. 2013.

[255] Zhihua Wang, Jun Tan, Qingze Zou, and Wei Jiang, "Control-based high-speed direct mask fabrication for lithography via mechanical plowing," in *2013 American Control Conference (ACC)*, 2013, pp. 5183–5188.

[256] M. Heyde, K. Rademann, B. Cappella, M. Geuss, H. Sturm, T. Spangenberg, and H. Niehus, "Dynamic plowing nanolithography on polymethylmethacrylate using an atomic force microscope," *Rev. Sci. Instrum.*, vol. 72, no. 1, pp. 136–141, Jan. 2001.

[257] X. Lu, C. Balocco, F. Yang, and A. M. Song, "Highly Reproducible Nanolithography by Dynamic Plough of an Atomic-Force Microscope Tip and Thermal-Annealing Treatment," *IEEE Trans. Nanotechnol.*, vol. 10, no. 1, pp.

53–58, Jan. 2011.
[258] C. Song, X. Li, B. Yu, H. Dong, L. Qian, and Z. Zhou, “Friction-induced nanofabrication method to produce protrusive nanostructures on quartz,” *Nanoscale Res. Lett.*, vol. 6, no. 1, pp. 310–319, Jan. 2011.
[259] R. García, R. Magerle, and R. Perez, “Nanoscale compositional mapping with gentle forces,” *Nat. Mater.*, vol. 6, no. 6, pp. 405–411, 2007.
[260] A. P. Nievergelt, J. D. Adams, P. D. Odermatt, and G. E. Fantner, “High-frequency multimodal atomic force microscopy,” *Beilstein J. Nanotechnol.*, vol. 5, pp. 2459–2467, 2014.
[261] D. J. Müller and Y. F. Dufrêne, “Atomic force microscopy as a multifunctional molecular toolbox in nanobiotechnology,” *Nat. Nanotechnol.*, vol. 3, no. 5, pp. 261–269, 2008.
[262] O. Schneegans, F. Houze, R. Meyer, and L. Boyer, “Study of the local electrical properties of metal surfaces using an AFM with a conducting probe,” *IEEE Trans. Components, Packag. Manuf. Technol. Part A*, vol. 21, no. 1, pp. 76–81, 1998.
[263] J. Alvarez, I. Ngo, M.-E. Gueunier-Farret, J.-P. Kleider, L. Yu, P. R. Cabarrocas, S. Perraud, E. Rouviere, C. Celle, C. Mouchet, and J.-P. Simonato, “Conductive-probe atomic force microscopy characterization of silicon nanowire,” *Nanoscale Res. Lett.*, vol. 6, no. 1, pp. 110–119, Jan. 2011.
[264] S. Jesse and S. V Kalinin, “Band excitation in scanning probe microscopy: sines of change,” *J. Phys. D. Appl. Phys.*, vol. 44, no. 46, pp. 464006–16, Nov. 2011.
[265] S. Xu and M. F. Arnsdorf, “Electrostatic force microscope for probing surface charges in aqueous solutions,” *Proc. Natl. Acad. Sci.*, vol. 92, no. 22, pp. 10384–10388, Oct. 1995.
[266] E. Van Der Pol, A. G. Hoekstra, A. Sturk, C. Otto, T. G. Van Leeuwen, and R. Nieuwland, “Optical and non-optical methods for detection and characterization of microparticles and exosomes,” *J. Thromb. Haemost.*, vol. 8, no. 12, pp. 2596–2607, Dec. 2010.